LNEC TRIAXIAL SEISMIC SHAKING TABLE
Notes related with the *tuning* of INSTRON actuator servocontrollers

F. J. Carvalhal, LNEC

Introductory remark: These notes are specially addressed to the members of the LNEC scientific and technical staff who are involved with the triaxial seismic shaking table supervision and operation. Thus, the main purpose of writing down these notes is to present the fundamental concepts concerned with what is usually called a servocontroller and to illustrate the effectiveness of the possible components of such a control scheme, namely the *AAF* (auxiliary acceleration feedback) and the *PID* (proportional plus integral plus derivative) controllers. As it is well-know from field experience, these kind of theoretical rationalisations are indeed important and helpful in the extent that they shall provide for the necessary insight and framework to cope with the tuning of the real servosystem.

1. Brief introduction

Each one of the axis of the LNEC triaxial seismic shaking table is driven by a position servocontrolled hydraulic actuator. Due to the design principles of the seismic table it is expected that there exists no cross-coupling between the three orthogonal axis. In view of this, the servocontrollers operate in an univariable manner (i.e., as a single input-single output system). So, despite the fact that the flow-control servovalves used on the vertical actuator are different from those pertaining to the transversal and the longitudinal ones, for the purpose of these notes we may take into consideration only one of the three axis.

2. System to be controlled

Bearing in mind that the servocontroller tuning procedure will be carried out using rigid masses (or dead-weights) – mounted upon the seismic table and with a total mass matching the mass of the test specimen – then we may consider that the system to be controlled is assembled by: *a)* an electrohydraulic flow-control servovalve plus a hydraulic cylinder (also called the actuator) and *b)* a rigid mass (or, again, a dead-weight) connected to the rod, as schematically depicted in Fig. 1.

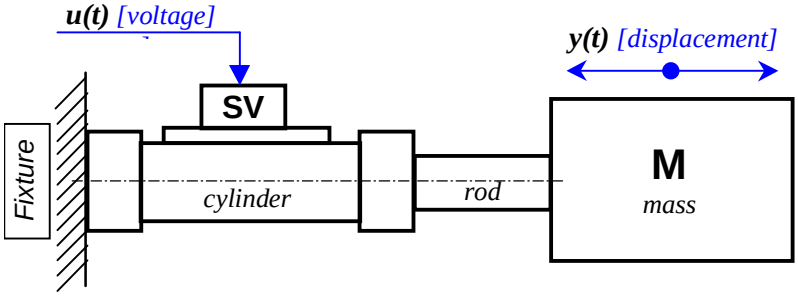

Figure 1 - System to be controlled (schematic representation)

Note that in this simplified approach we assume the existence of ("infinitely") rigid connections between the actuator body and the fixture (a quite reasonable assumption) as well as between the actuator rod and the driven mass (not so much a reasonable assumption, in the case

of the LNEC seismic table, but still acceptable within the scope of these notes). In Fig. 2 it is shown the corresponding block diagram

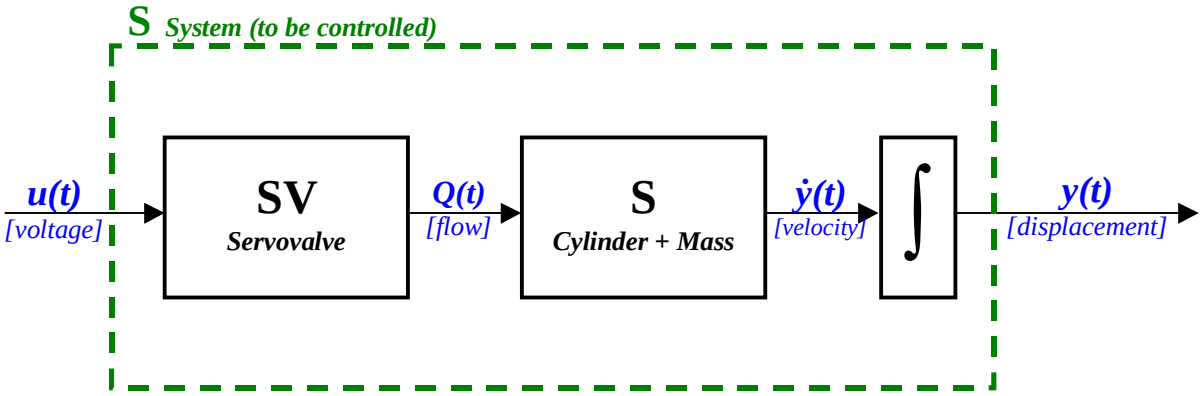

Figure 2 - System to be controlled (block diagram)

where *u(t)* denotes the system input (electrical voltage, or current, which is fed to the servovalve first stage: the torque motor), *y(t)* the system output (actuator rod or moving mass position or displacement), *Q(t)* the oil flow entering the cylinder chambers and $\dot{y}(t)$ the actuator rod velocity. Note that this is a Type 1 system, meaning (in control theory jargon) that for a constant input we shall have a constant rate of variation (first time-derivative) of the output or, in other words, for this particular case, a constant voltage fed to the servovalve will result in a constant oil flow and, therefore, a constant velocity of the actuator rod; this accounts for the presence of the integrator block ($y(t) = \int \dot{y}(t)\, dt$).

2.1 - System transfer function

Assuming that the system is linear, we may consider its input-output dynamical relationship as represented by the so-called *transfer function*. In this case, this kind of mathematical model can be written as follows:

$$G_S(s) = \frac{Y(s)}{U(s)} = \frac{K_S.(\omega_{SV1}.\omega_{SV2}^2.\omega_S^2)}{s\,(s+\omega_{SV1})\,(s^2+2\zeta_{SV2}\omega_{SV2}s+\omega_{SV2}^2)\,(s^2+2\zeta_S\omega_S s+\omega_S^2)} \qquad (1)$$

where K_S denotes the system d.c. gain, i.e. the relationship between output *y* and input *u* in the steady-state (in our case, this gain has the units of velocity per electrical voltage or current). In the function denominator we have the integrator, a first order lag and a quadratic lag, both due to the servovalve, and another quadratic lag, due to the cylinder plus driven mass. To model the servovalve dynamics it could be used just one quadratic lag, but for three-stage servovalves (as we have in both the transversal and longitudinal axis) we consider that this is a more adequate model. The complex variable *s* ($= \sigma + j\omega$) is often called the Laplace variable; note that by replacing *s* by $j\omega$ we shall obtain the well-known system *frequency response function* (FRF).

The values of ω_{SV1}, ω_{SV2} and ζ_{SV2} depend solely on the servovalves characteristics and thus they have to be estimated based on technical specifications provided by the respective manufacturer (by MOOG, in our case).

The value of K_S has a combined dependence on the characteristics of both the servovalve and the actuator (hydraulic cylinder). For a flow-control electrohydraulic servovalve we may admit that the output oil flow is proportional to the electrical input voltage (or current). Then we may say that there exists a gain K_{SV}, the servovalve flow gain (flow units per voltage units); the value of this gain is supplied by the servovalve manufacturer. As an approximation, we may also admit that this gain is equal to the servovalve rated flow (flow that produces a pressure drop of 1000 psi across the servovalve ports) divided by the input voltage value that causes the maximum valve opening (100% command signal). On the other hand, we still may say that there is also a gain K_C, that we might call the cylinder gain (velocity units per flow units). Knowing that the rod velocity is equal to the flow entering one of the two cylinder chambers, $Q(t)$, divided by the piston effective area, A, then $y,^{\cdot}(t) = Q(t)/A = Q(t).K_C$, and thus $K_C = 1/A$. Consequently, we have

$$K_S = \frac{K_{SV}}{A} \tag{2}$$

Finally, the values of ω_S and ζ_S depend on the hydraulic cylinder geometric characteristics (stroke and piston effective area), on the value of the driven rigid mass and on the oil characteristics (namely the oil *bulk modulus*, which relates to the "stiffness" of the liquid). However, since our system is not effectively a rigid mass those values also depend on other physical features such as compliance and damping effects of several system mechanical components.

Taking into account that our system has two types of servovalves and two types of actuators arranged in different configurations and, above all, the main purpose of these notes, we will assume not only K_S =1 but also the following reference or typical values regarding natural frequencies and damping ratios

ω_{SV1} = 502.65 rad/s (≈ 80 Hz)
ω_{SV2} = 251.33 rad/s (≈ 40 Hz)
ζ_{SV2} = 0.6
ω_S = 62.83 rad/s (≈ 10 Hz)
ζ_S = 0.2

So, from expression 1, we will assume the following system transfer function

$$G_S(s) = \frac{(502.65 \times 63165.47 \times 3947.84)}{s\,(s+502.65)\,(s^2+301.59\,s+63165.47)\,(s^2+25.13\,s+3947.84)} \tag{3}$$

that has no zeros but has the following six poles

0
-502.65
-150.80 + *j* 201.06
-150.80 – *j* 201.06
-12.57 + *j* 51.66
-12.57 – *j* 51.66

Nevertheless, note that most probably the value of ω_S will be lower than the assumed 10 Hz; thus, some results obtained with ω_S = 9.42 rad/s (≈ 1.5 Hz) are attached at the end of these notes.

3. Servosystems

We could certainly wish that this system would dynamically behave like an ideal *servosystem*. Such an ideal system is essentially characterised by the following input-output dynamical time-domain relationship

$$y(t) = K.u(t) \tag{4}$$

within the frequency range of interest (generally, $[\omega_1,\omega_2]$); such a system would present, within that range, the frequency response depicted in Fig. 3. Once again, we should like to emphasise that this is an ideal situation.

By observing expression 1 (or likewise expression 3) we may conclude that this is not clearly our case. In fact, we may expect that our system will typically have a frequency response such as the sketch shown in Fig. 4.

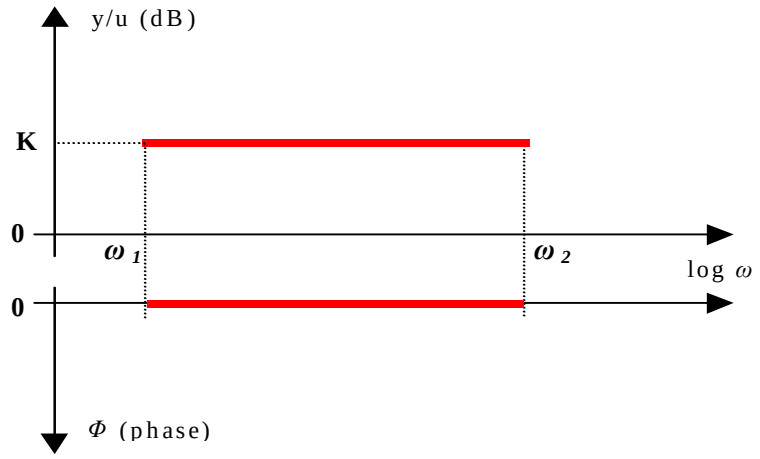

Figure 3 - Ideal frequency response of a servosystem

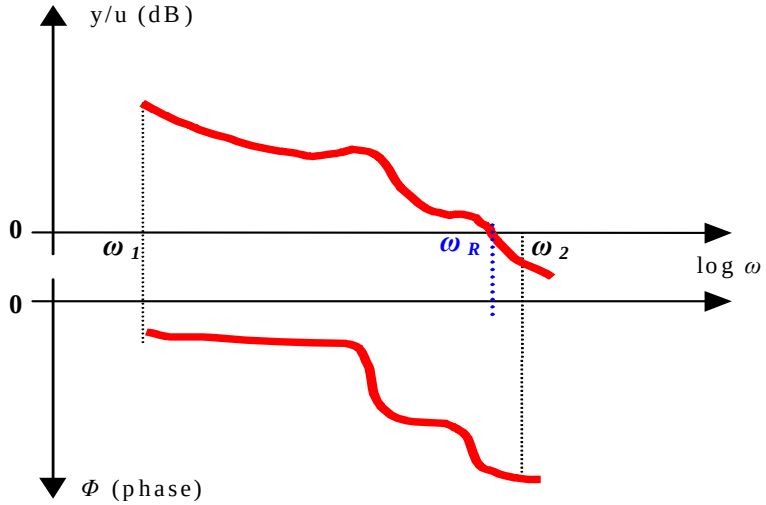

Figure 4 - Typical frequency response of our system (sketch)

Being so, it is then required to apply a control scheme to the system so that the resulting one would approximately behave like a servosystem. The implementation of such a control scheme give rise to what is commonly called a *servocontroller*.

The use of the word "approximately" deserves a brief comment, expressly in what regards the type of system that we are currently examining. In effect, the LNEC triaxial seismic table operates hinging on a self-tuning (also called adaptive) outer control loop (by using the computer program SPiDAR), which, after a certain number of iterations – taking into due account the estimated frequency response of the overall servocontrolled system (and this in a multivariable manner) –, computes the input that shall produce an output very close to the desired one (the *target*, that, after all, is the seismic excitation to which we require to subject the test specimen).

So, the degree of "flatness" of the servosystem frequency response should not be our major concern when dealing with its tuning. In terms of frequency response, our major goal shall be to ensure (if that is possible) that the system bandwidth encompasses the frequency range of interest; that is to say, that $\omega_R > \omega_2$, being $\omega_1 = 0$ (see Fig. 4), without jeopardising the system relative stability (recall the concepts of *gain margin* and of *phase margin* used in the Bode analysis of control systems).

4. The servocontroller

The implemented INSTRON closed-loop position servocontroller has three main components (or controllers): *a)* a *PID* controller, *b)* an auxiliary acceleration feedback (*AAF*) controller, and *c)* a lag controller. Presently, there is no sufficient data about the technical specifications of those control components.

Disregarding, at least for the moment, the lag controller, it is possible however to make an educated guess about the main characteristics of the other two servocontroller components. In other words, we shall examine a servocontroller scheme that we assume to be close enough to the existent INSTRON servocontroller.

Firstly, we may expect that the block diagram should be as the one shown in Fig. 5. Needless to say, it is important to pay attention to this diagram, including the used notation and terminology.

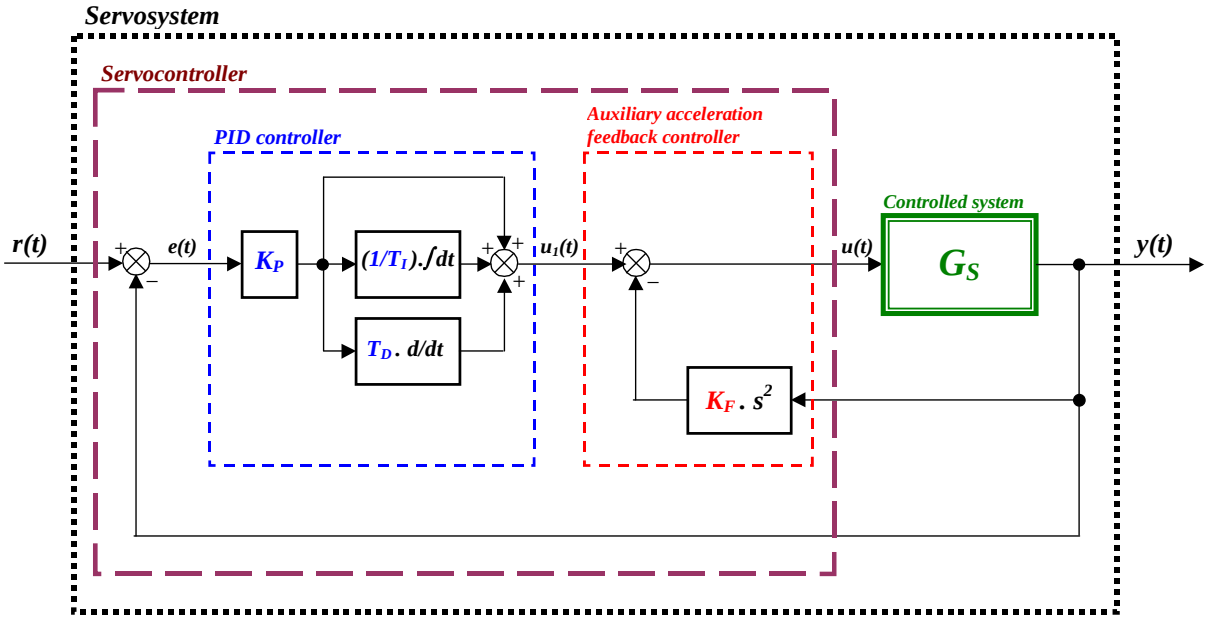

Figure 5 - Servocontroller block diagram (assumed)

We have then four parameters to change in order to tune the servosystem, three of them belonging to the *PID* controller:

K_P	the proportional gain (expressed in dB),
T_D	the derivative gain (in milliseconds, ms),
$1/T_I$	the integral gain (in s^{-1}),

and the fourth pertaining to the auxiliary acceleration feedback controller:

K_F	the auxiliary feedback gain (dimensionless).

4.1 - The auxiliary acceleration feedback (*AAF*) controller

The auxiliary acceleration feedback (*AAF*) controller is in fact an inner loop. When this loop is closed (i.e. when $K_F > 0$) we may consider that the controlled system transfer function has been modified from $G_S(s)$ to $G_{Sm}(s)$ as schematically depicted in Fig. 6.

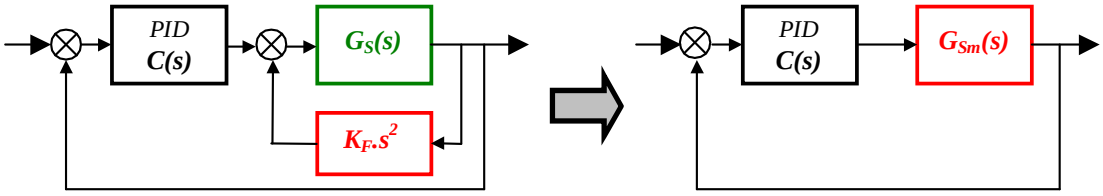

Figure 6 - *AAF* applied to the system to be controlled

The modified controlled system transfer function is then given by the following expression

$$G_{Sm}(s) = \frac{G_S(s)}{1 + K_F.s^2.G_S(s)} \tag{5}$$

and we may notice that, as expected, $G_{Sm}(s) \neq G_S(s)$ unless $K_F = 0$.

It is important to understand the effects that are obtained when a *AAF* controller is applied to a system like the one we are considering, that is to say, to a system characterised by a transfer function quite similar to the one of expression 1.

This can be accomplished resorting to the so-called *root locus* technique. But, beforehand, it may prove to be helpful to recall a few basic aspects closely related with this technique, frequently used in the analysis and synthesis of control systems.

4.1.1 - *Recalling a few root locus basic aspects*

When we use this technique, we begin by plotting in the complex plane the poles (roots of the denominator) and the zeros (roots of the numerator) of the open-loop transfer function $GH(s) = G(s).H(s)$, where $G(s)$ denotes the feedforward path transfer function (obtained by multiplying all the block transfer functions lying in cascade on that path) and $H(s)$ stands for the feedback path transfer function (obtained in a similar way). That open-loop transfer function implicitly includes the open-loop gain factor, K, that we assume to have a value that may be varied. Usually, the poles are depicted by small crosses (×) and the zeros are depicted by small circles (o). The branches that depart from the poles and arrive at the zeros or the infinity

represent the placement of the poles of the closed-loop transfer function when the open-loop gain factor varies from zero to infinity (or, in practice, to a number as large as we may wish); in other words, we obtain the closed-loop pole-zero map. Both poles and zeros can be either real or complex; if they are complex then they exist in conjugate pairs (i.e., having the same real part and symmetrical imaginary parts).

Let us now consider an underdamped second-order system. For such a system we have a transfer function with two poles corresponding to a quadratic lag: ($s^2 + 2\zeta\omega_n\, s + \omega_n$), where ω_n is called the (undamped) *natural frequency* and ζ the *damping ratio* ($0 \leq \zeta \leq 1$). The poles are given by

$$s = -\zeta\omega_n \pm j\,\omega_n\sqrt{1-\zeta^2} = -\sigma \pm j\omega_d \tag{6}$$

where $1/\sigma$ is called the system *time constant* and ω_d is called the *damped natural frequency*.

By observing Fig. 7 we may notice that the poles of these kind of simple systems having the same natural frequency ω_n but different damping ratios will be located on the depicted half circumference of radius ω_n. We may also notice that, for the same natural frequency, the closer the poles are to the imaginary axis, the lower is the damping ratio value and, conversely, that the closer they are to the negative real axis the higher is the damping ratio. Moreover, poles placed at a greater distance from the origin have higher natural frequencies.

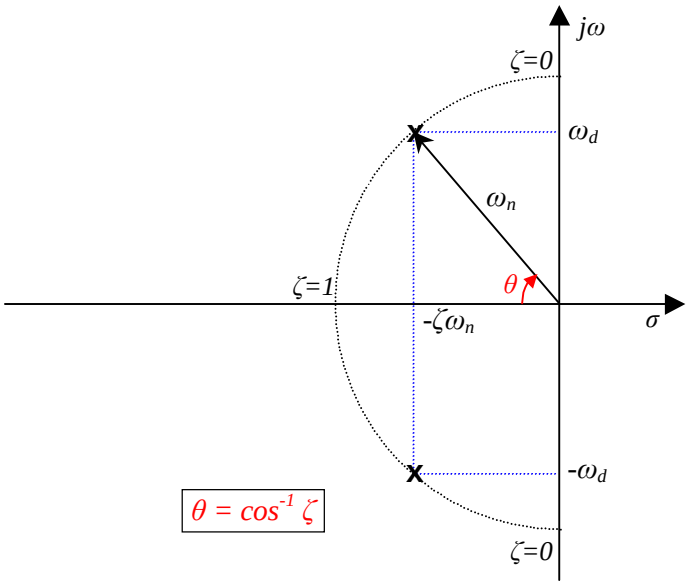

Figure 7 - Representing a pair of complex poles

The system time-response (to a step input function, for instance) depends on the real part absolute value (σ) of the poles and on the values of the *residues* at each one of them (the residues depend on the other poles and zeros). For each pole, the transient term of the response decays, according to $e^{-\sigma t}$, as rapidly as larger is σ. On the other hand, the value of the residue indicates the relative effect of the respective pole on the system total time-response; for the complete set of residues (as many as the number of poles), those having higher relative absolute values correspond to the poles that have greater contribution to the total time-response.

So, the system time-response tends to be "dominated" by the poles lying near the imaginary axis; therefore, if a system has a transfer function with one or two poles "isolated" on that zone they are usually called the *dominant* poles, in the sense that the system time-response greatly depends on their characteristic values. Nonetheless, we also have to bear in mind that if a zero is positioned in the vicinity of a pole than the influence of this pole is greatly reduced (near-cancellation effect).

Finally, let us recall that if at least one of the transfer function poles is placed in the right side of the complex plane (positive real part) then the system is unstable since its time-response shall be unbounded when time increases.

4.1.2 - *Main effects of AAF control action*

In order to understand the effects that are obtained when a *AAF* controller is applied to a system like the one we are considering, that is to say dynamically characterised by the transfer function given by expression 3, let us plot and examine the root loci obtained for different relative pole placement.

As we just said, $G_S(s)$ is given by expression 3, and $H(s) = K_F .s^2$ (see Fig. 6). Bearing in mind that $GH(s) = G_S(s).H(s)$, we then have

$$GH(s) = \frac{(502.65 \times 63165.47 \times 3947.84).K_F \; s^2}{s\,(s+502.65)\,(s^2+301.59\,s+63165.47)\,(s^2+25.13\,s+3947.84)} \tag{7}$$

or,

$$GH(s) = \frac{(\omega_{SV1} \times 63165.47 \times 3947.84).K_F \; s}{(s+\omega_{SV1})\,(s^2+301.59\,s+63165.47)\,(s^2+25.13\,s+3947.84)} \tag{8}$$

where it is relevant to notice that one of the two zeros from $H(s)$ located at the origin has cancelled with the system pole at the same location.

In Fig. 8, the superimposed root loci obtained to five different values to ω_{SV1} (case 1), 50.0 (red line), 200.0 (black line), 331.8 (blue line), 350.0 (magenta line) and 502.65 (green line) rad/s, are shown. Note that the zero at the origin as well as the two pairs of complex poles corresponding to the two quadratic lags are represented in this figure (one circle and four crosses, in black); however, the first order lag pole, lying on the real axis (on five different locations, corresponding to the different values of ω_{SV1}), is not graphically represented.

Also, be aware that these root loci result from varying the above-mentioned auxiliary feedback gain, K_F (so, we associate this gain with the open-loop gain factor).

Just for the sake of easing the task of understanding that figure, the root locus for each one of the five situations are individually shown in figures 9 to 13.

By observing Fig. 8, we see that those loci drastically change with the value of ω_{SV1}, going from the configuration in red (lowest value of ω_{SV1}) to the one in green (highest value of ω_{SV1}), including a transition configuration corresponding to the locus in blue.

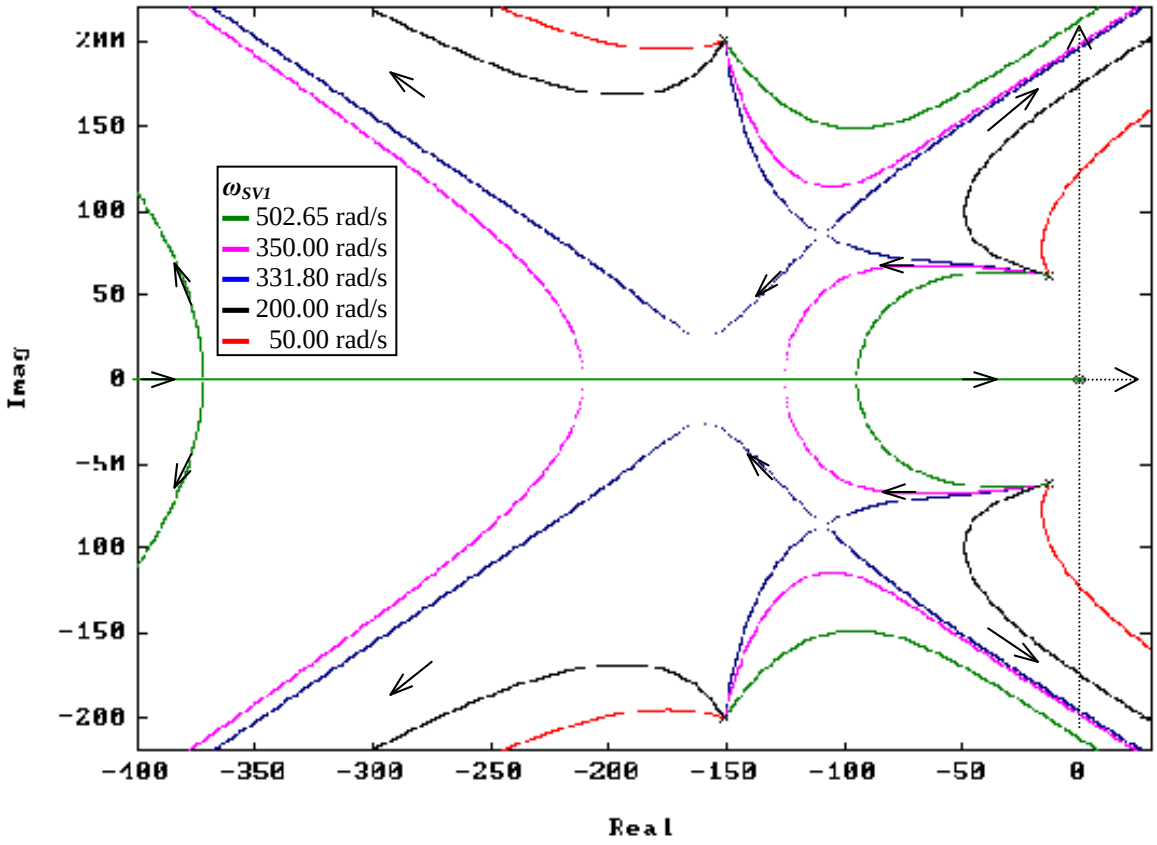

Figure 8 - Superimposed root loci of system with *AAF* (case 1)

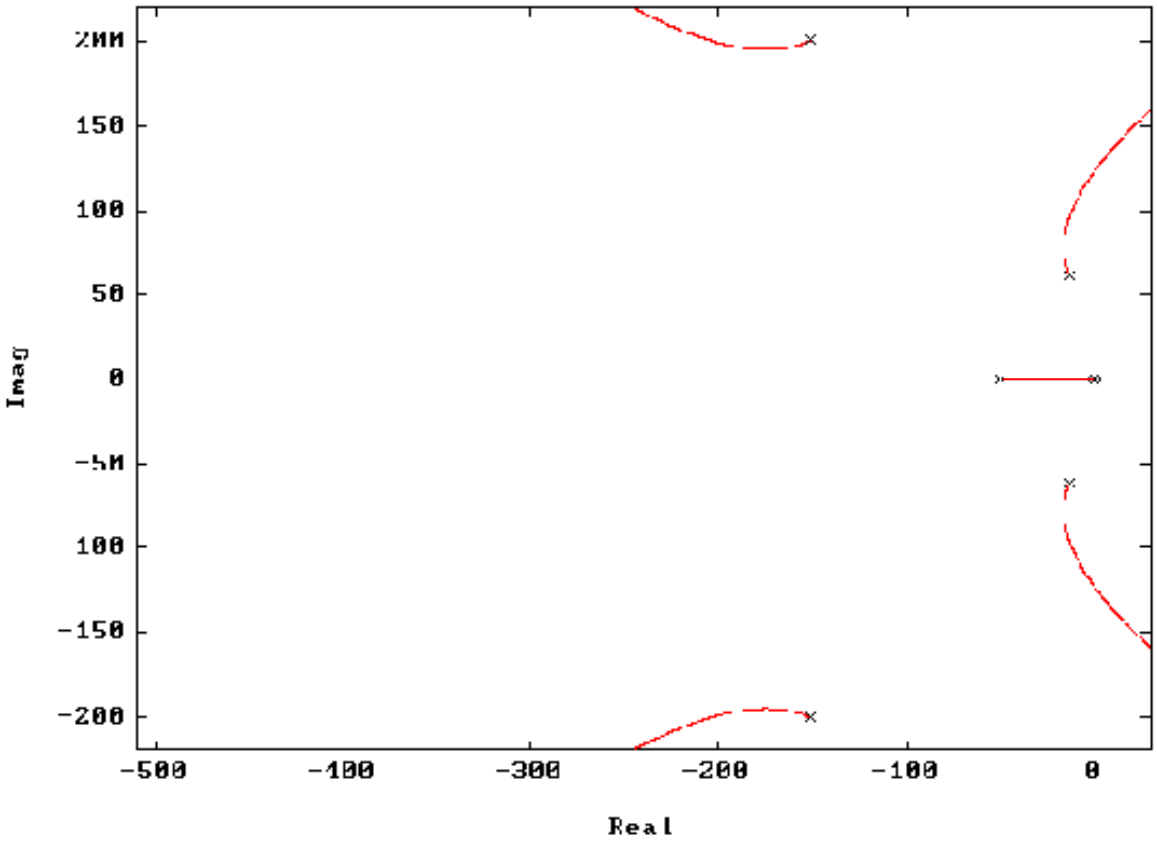

Figure 9 - Root locus of case 1 with ω_{SV1}=50.0 rad/s

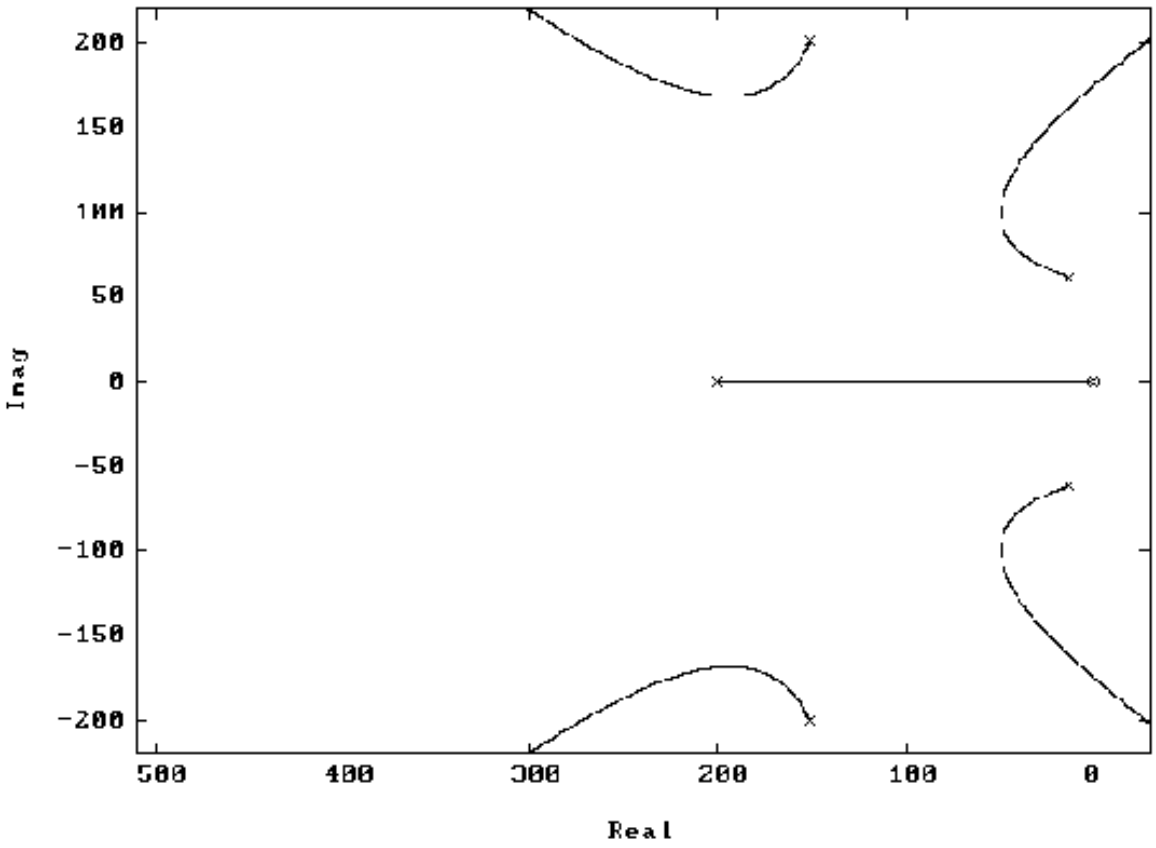

Figure 11 - Root locus of case 1 with ω_{SV1}=200.0 rad/s

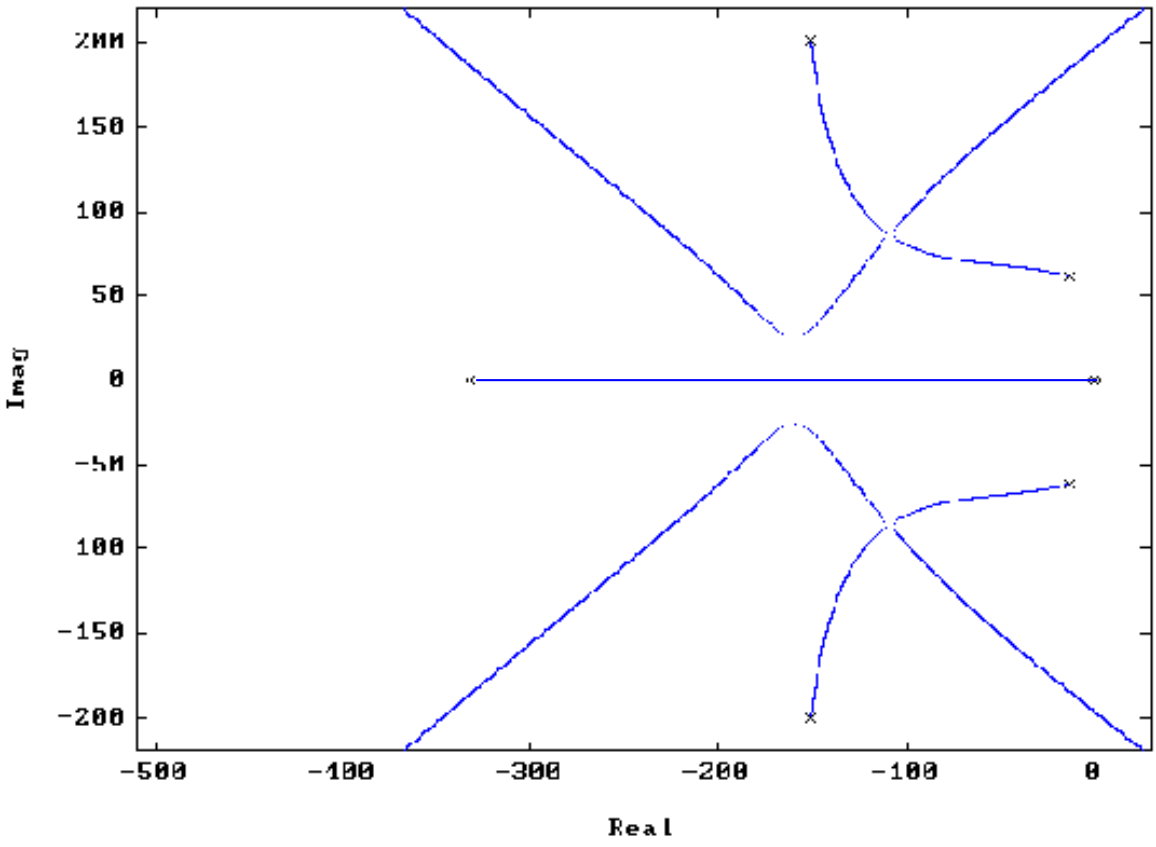

Figure 10 - Root locus of case 1 with ω_{SV1}=331.8 rad/s

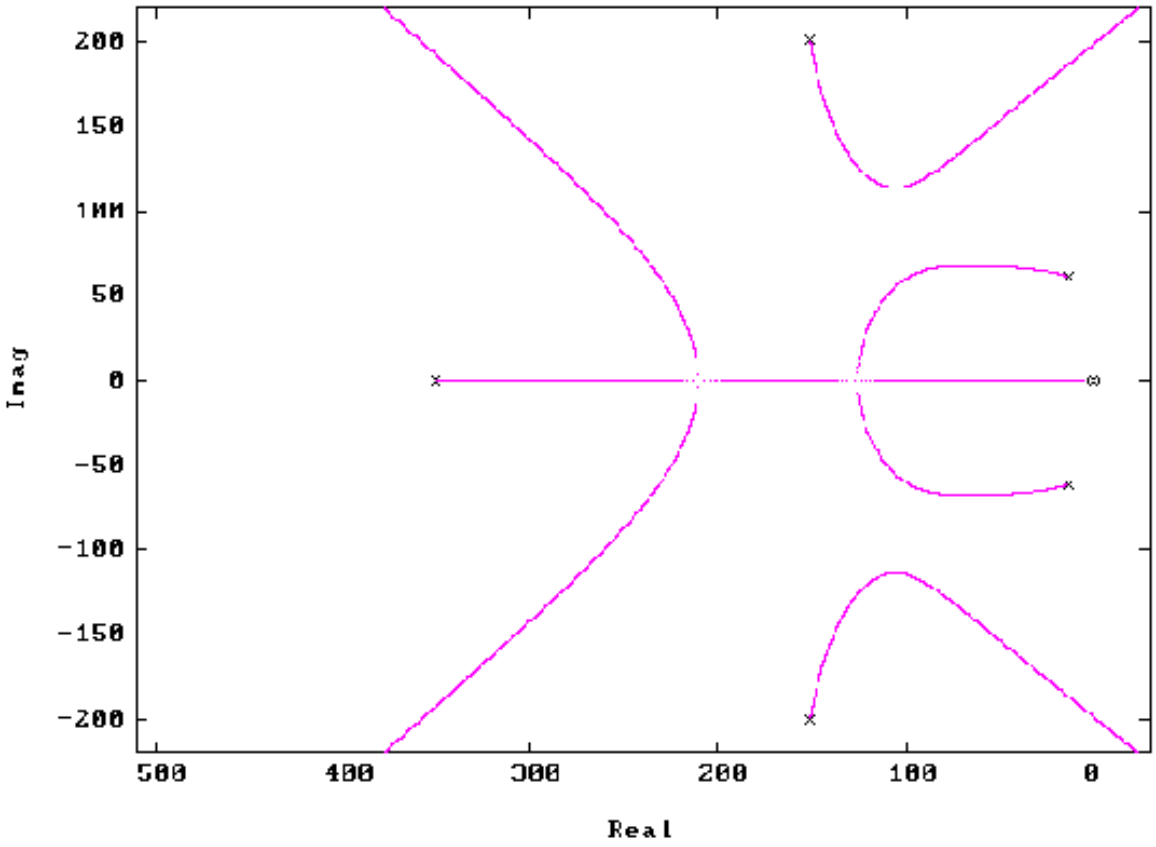

Figure 11 - Root locus of case 1 with ω_{SV1}=350.0 rad/s

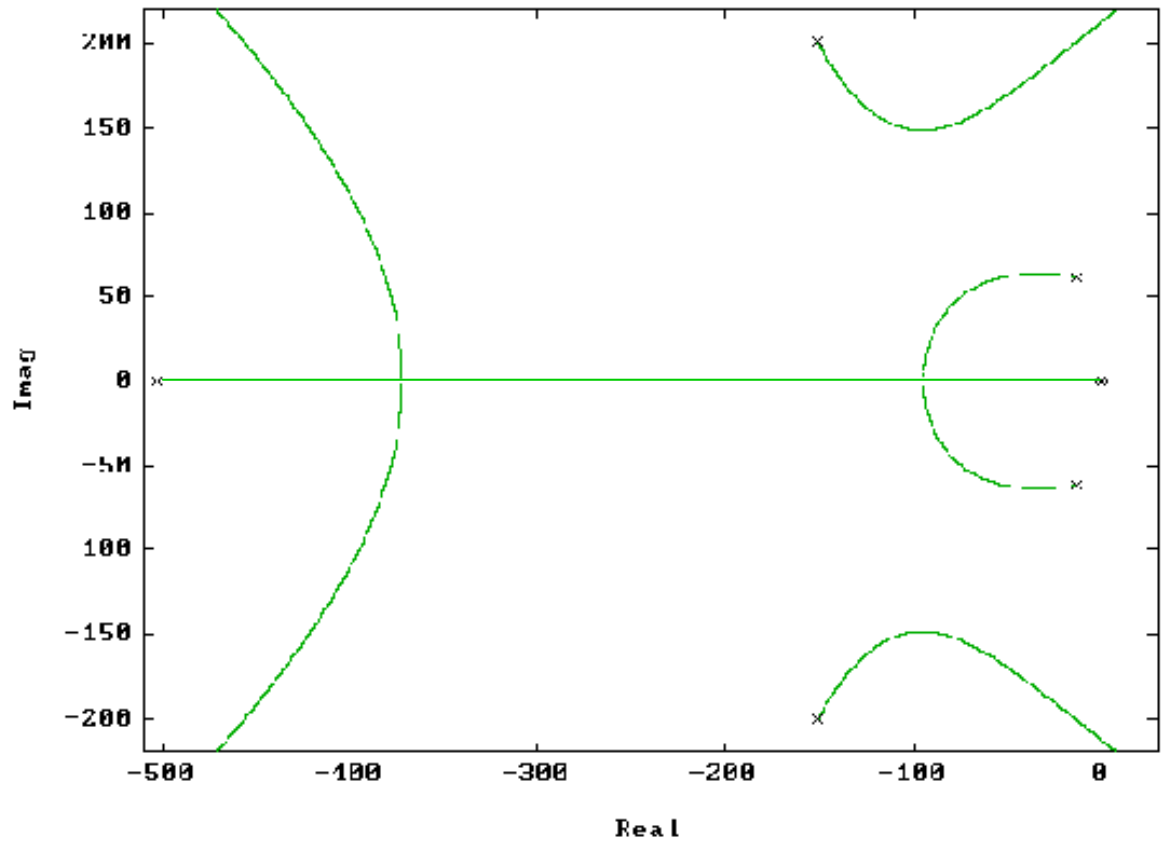

Figure 12 - Root locus of case 1 with ω_{SV1}=502.65 rad/s

In Fig. 13 the superimposed root loci for another case (case 2) are shown. As we did previously with respect to case 1, the root locus for each one of these four situations are individually shown in figures 14 to 17.

In case 2, the value of ω_{SV1} was kept constant and equal to 502.65 rad/s and the complex poles located far to the left of the imaginary axis (the pair corresponding to ω_{SV2} and to ζ_{SV2}) were sequentially displaced towards the right side, thus approaching the other pair of complex poles placed near of that axis (sequence green, blue, black, red).

By observing Fig. 13, we see that if the complex poles located on the left side are sufficiently close to the complex poles located near the imaginary axis, then the branches leaving from the latter almost immediately go towards the right-side of the complex plane, in a very similar way to the one observed to the case 1; thus, the desired effect of using an *AAF* controller is drastically reduced or even non-existent.

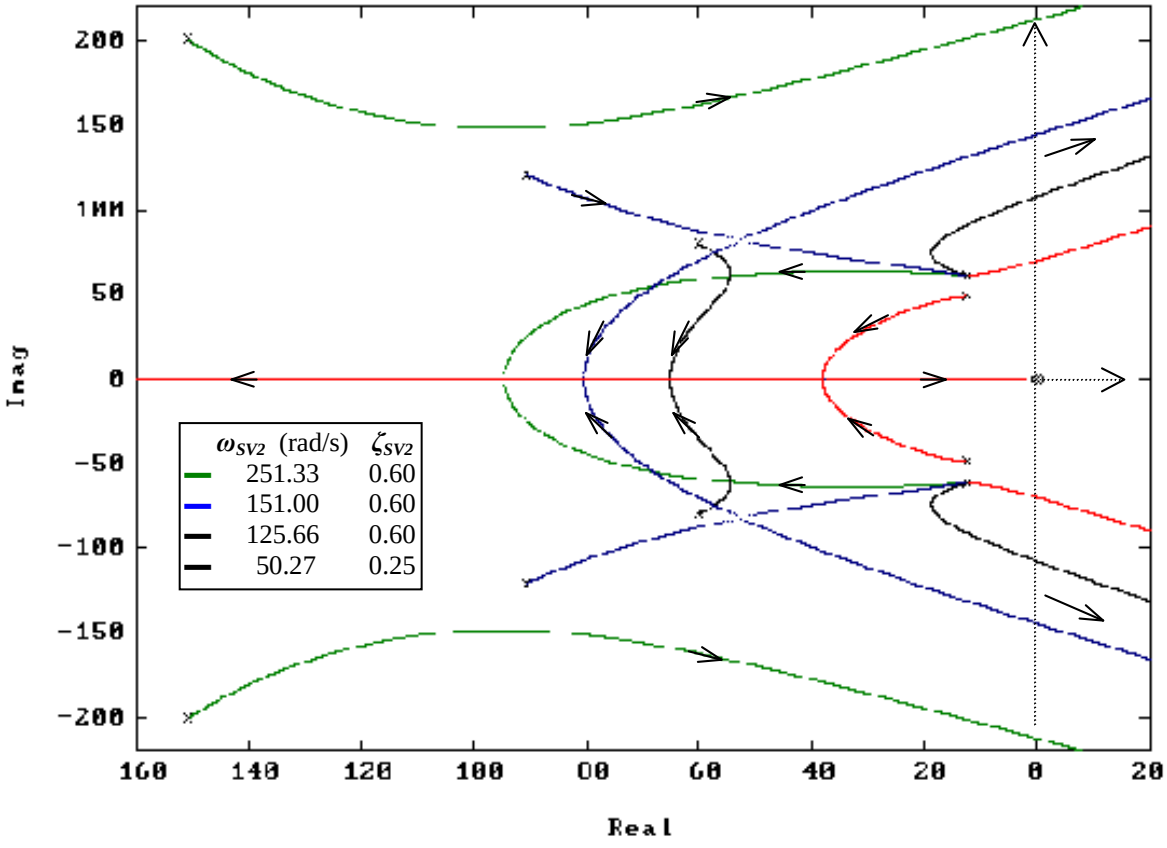

Figure 13 - Superimposed root loci of system with *AAF* (case 2)

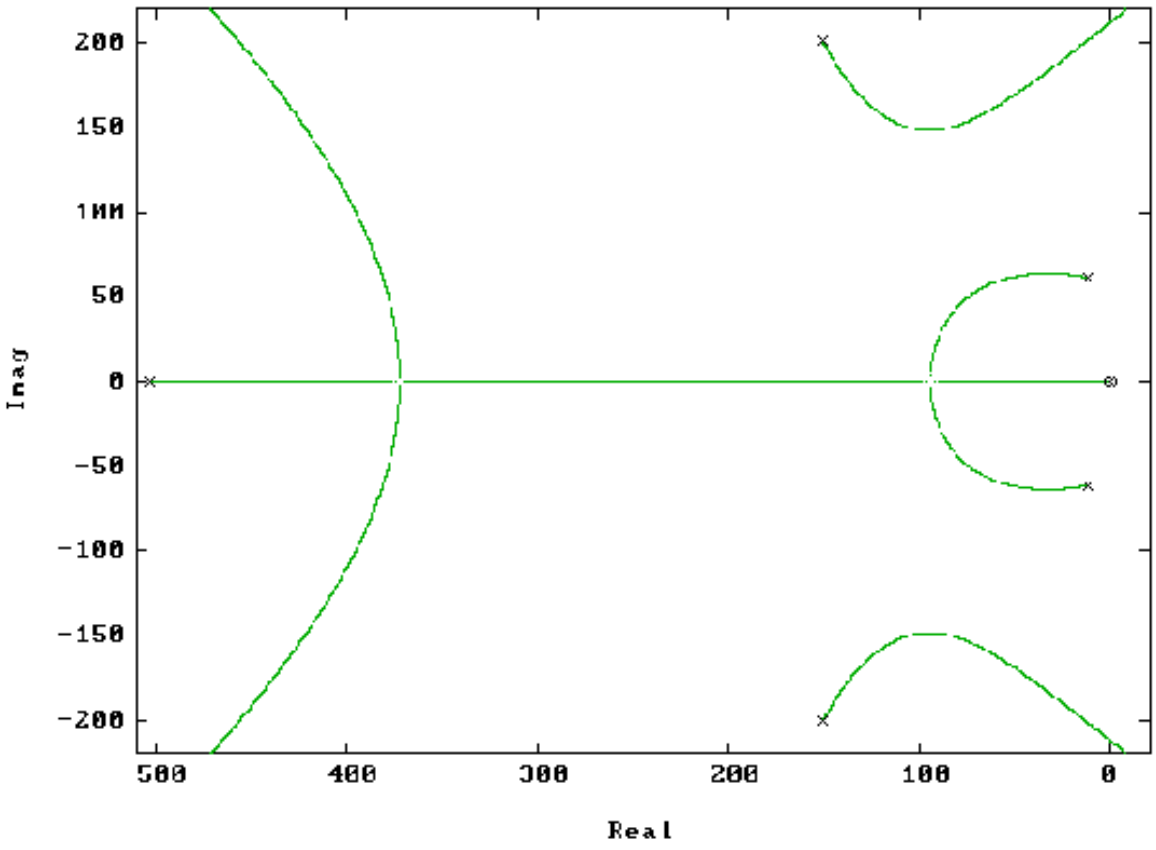

Figure 14 - Root locus of case 2 with ω_{SV1}=251.33 rad/s and ζ_{SV2}=0.6

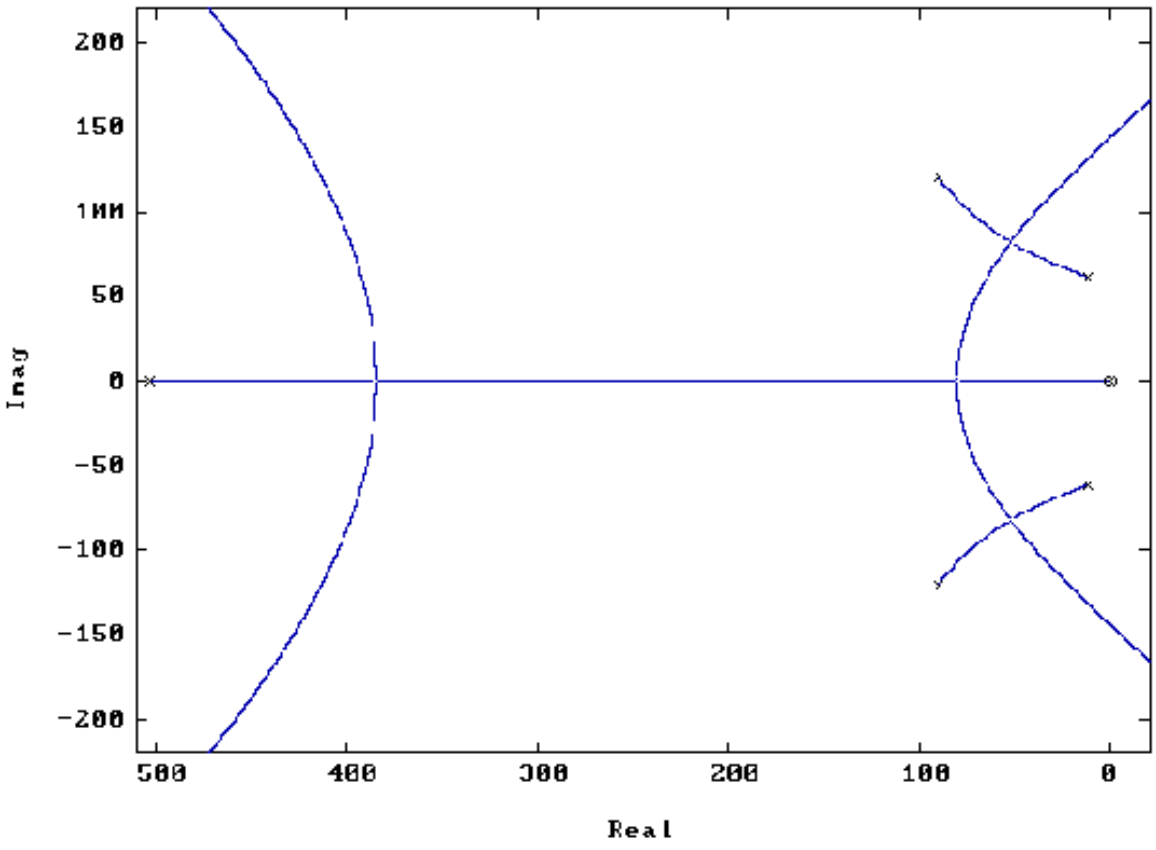

Figure 15 - Root locus of case 2 with ω_{SV1}=151.0 rad/s and ζ_{SV2}=0.6

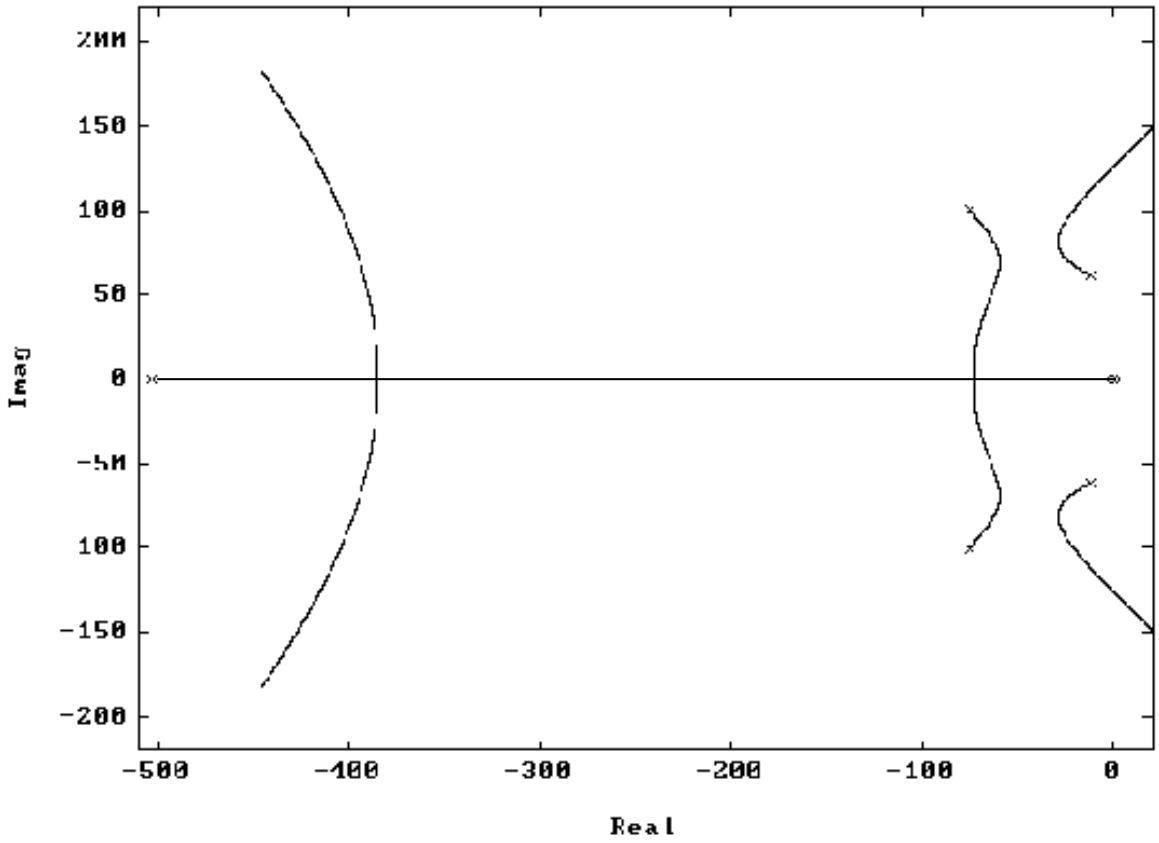

Figure 16 - Root locus of case 2 with ω_{SV1}=125.66 rad/s and ζ_{SV2}=0.6

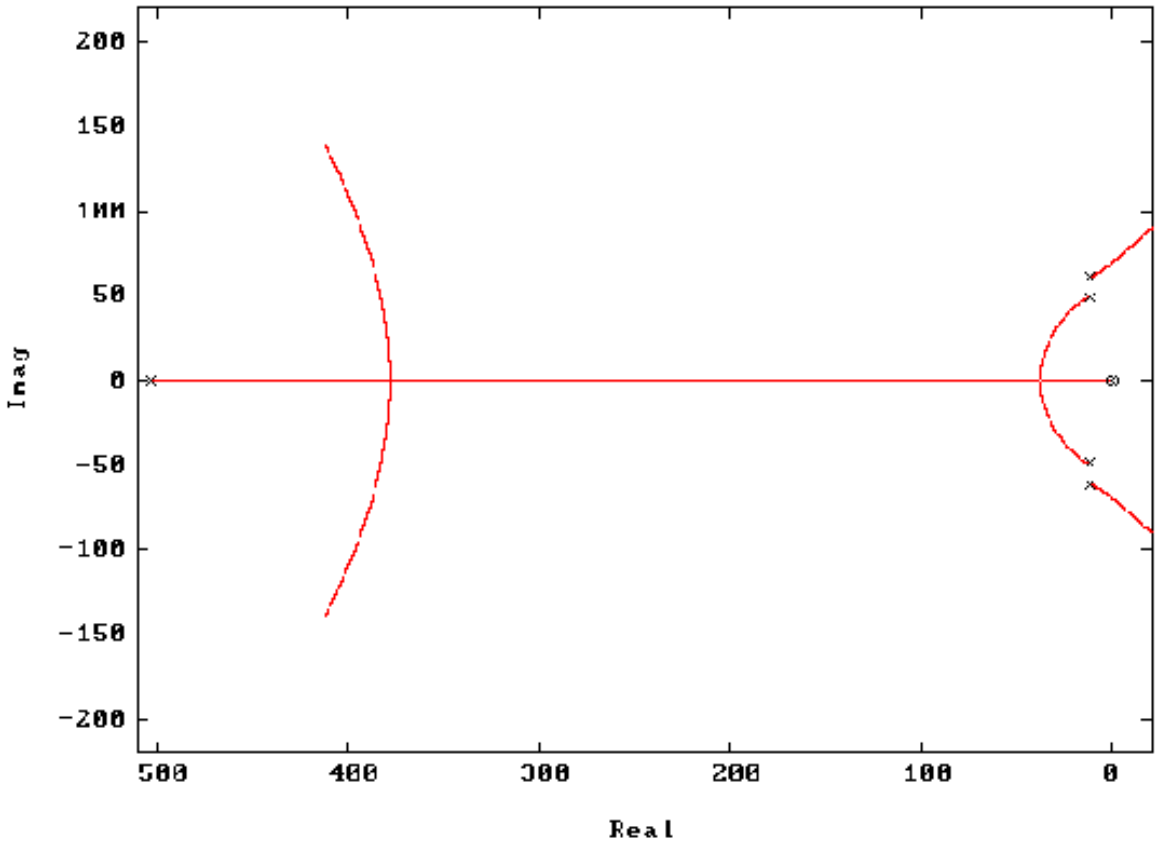

Figure 17 - Root locus of case 2 with ω_{SV1}=50.27 rad/s and ζ_{SV2}=0.25

4.1.3 - *Some closing comments about the AAF control action*

Taking these examples into account, we may conclude that, essentially, the use of an *AAF* controller (when applied to a system characterised by a transfer function very similar to the one of expression 1) will possibly allow, depending on the relative location of the system poles, and by setting a suitable value of K_F, the placement of the dominant complex poles farther to the left of the imaginary axis, thus increasing the relative stability of the system; moreover, it will also permit, in some situations, an increase of the damping ratio and/or of the natural frequency associated with those dominant poles. Hence, if that will be the case, when closing the position feedback loop, that increase of relative stability will generally allow, in turn, the increase of the system bandwidth.

In Fig. 18 it is shown the root locus (branches in green departing from poles represented by small crosses in black) using *AAF* control applied to the system we have been considering, whose transfer function $G_S(s)$ is given by expression 3. The small blue and red dots represent the poles location for $K_F = 0.01$ and for $K_F = 0.02$, respectively. Note the pole at the origin (red/blue); it will stay there regardless of the K_F value.

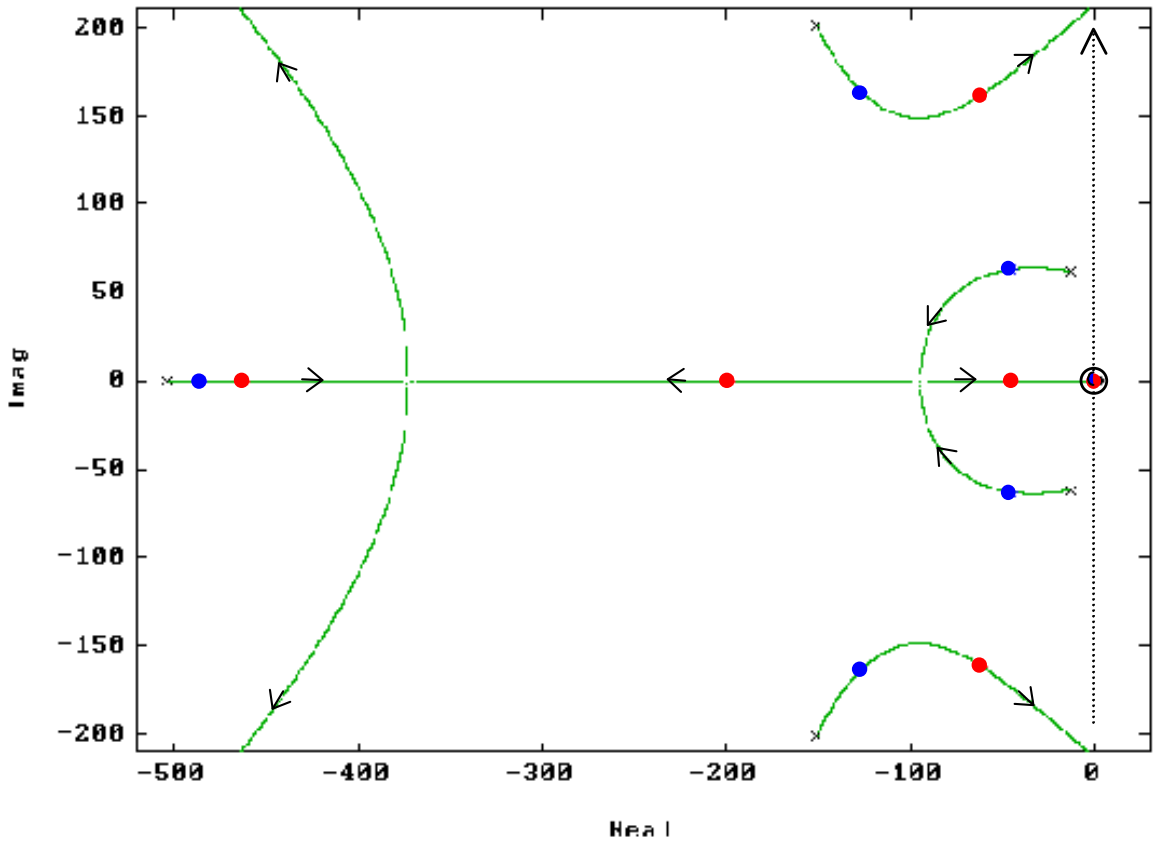

Figure 18 - Root locus of $G_S(s)$ with *AAF*

As a final comment about the *AAF* controller, it has to be stressed that the desired effects (an increase of relative stability and, as a possible consequence, of the damping ratio and/or of the natural frequency associated with the dominant complex poles) expected through its use will significantly depend on the dynamic characteristics of the system to which it is applied (i.e. on the relative location of the system transfer function poles and zeros). Thus, in our case, care must be exercised in using and tuning it.

4.2 - The *PID* controller

Let us now examine the *PID* controller action. For this purpose, we may or may not assume that the *AAF* control loop is closed. In either case, we are still examining the situation depicted in the right part of Fig. 6; if the *AAF* loop is open then $G_{Sm}(s) = G_S(s)$.

Assuming the *PID* structure shown in Fig. 5, we have

$$u_1(t) = K_P.\left(e(t) + T_D \frac{d\ e(t)}{dt} + \frac{1}{T_I}\int e(t)\ dt \right) \tag{9}$$

and, by using the Laplace transform,

$$U_1(s) = K_P\left[E(s) + T_D\ s\ E(s) + \frac{1}{T_I}\frac{E(s)}{s} \right] \tag{10}$$

we obtain the *PID* transfer function

$$C(s) = C_{PID}(s) = \frac{K_P\left(T_D\ s^2 + s + \frac{1}{T_I} \right)}{s} \tag{11}$$

that can be rewritten as

$$C(s) = C_{PID}(s) = \frac{K_P\ (s - z_1)(s - z_2)}{s} \tag{12}$$

where

$$z_1 = -\frac{1}{2T_D} + \frac{1}{2T_D}\sqrt{1 - 4T_D\frac{1}{T_I}} \quad \text{and} \quad z_2 = -\frac{1}{2T_D} - \frac{1}{2T_D}\sqrt{1 - 4T_D\frac{1}{T_I}} \tag{13}$$

Thus, the *PID* controller is basically characterised by a transfer function with one pole at the origin and two zeros lying in the real axis, if $4T_D/T_I \leq 1$, or as a complex pair, otherwise.

In some cases, it is usual to disregard either the derivative action or the integral action, giving rise, respectively, to the so-called *PI controller* ($T_D = 0$) or to the *PD controller* ($1/T_I = 0$). For these particular controllers we have the following transfer functions

$$C_{PI}(s) = \frac{K_P\ (s + 1/T_I)}{s} \tag{14}$$

$$C_{PD}(s) = K_P\ T_D\ (s + \frac{1}{T_D}) \tag{15}$$

Obviously, if T_D and $1/T_I$ are both set to zero the *PID* controller becomes just the classical and simpler feedforward path controller (or cascade compensator): the *proportional gain*.

Now the question resolves itself into this: given the dynamic characteristics of $G_{Sm}(s)$, what are the more suitable values of K_P, T_D and $1/T_I$ in order to attain the required control strategy, which, in our case, could be to increase the system bandwidth without loosing the adequate margin of relative stability.

Amongst the several approaches that can be used to examine this issue, we shall resort again to the root locus technique, bearing in mind what we have just said, that is to say, that our primary (although not the only one) goal will be to widen the system bandwidth.

To begin with, we shall consider four characteristic *PID* control configurations as depicted on Fig. 19, where red crosses or small red circles represent the poles or zeros, respectively, of the *PID* controller and black crosses stand for the poles of the system to which it is applied.

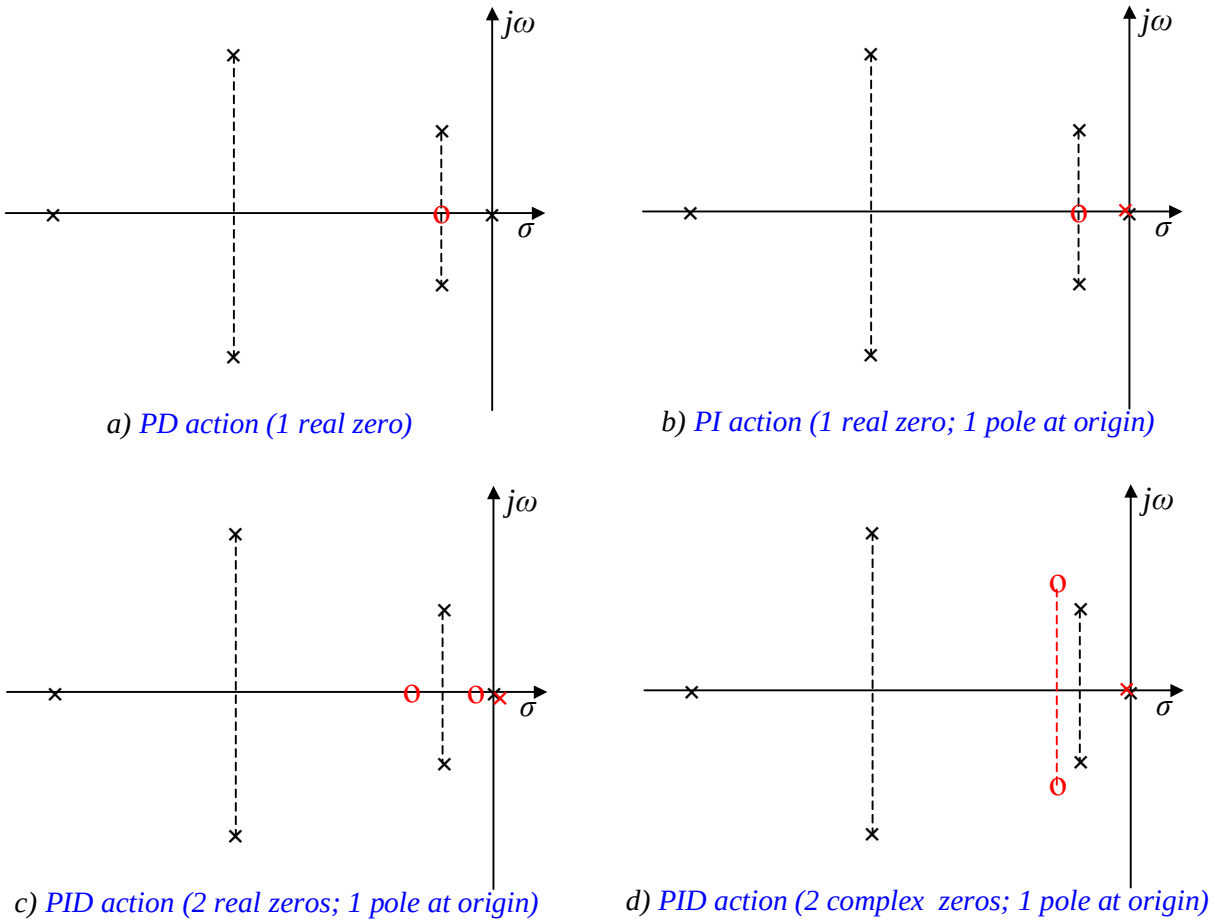

a) PD action (1 real zero)

b) PI action (1 real zero; 1 pole at origin)

c) PID action (2 real zeros; 1 pole at origin)

d) PID action (2 complex zeros; 1 pole at origin)

Figure 19 - Four characteristic PID control configurations

Moreover, we shall also continue to take into account the same system that has been considered so far and thus the PID control action will be applied to a system with a transfer function $G_S(s)$ given by expression 3 which we present once again

$$G_S(s) = \frac{(502.65 \times 63165.47 \times 3947.84)}{s\,(s+502.65)\,(s^2+301.59\,s+63165.47)\,(s^2+25.13\,s+3947.84)}$$

Before we proceed, it is most convenient to recall that we are dealing with a situation such as the one schematically shown in Fig. 20.

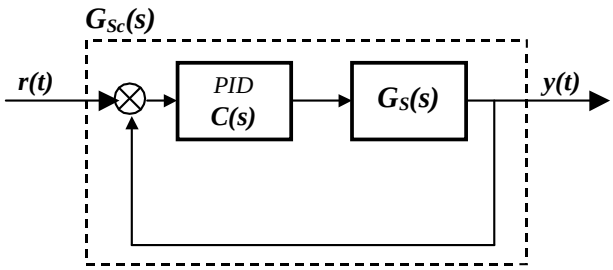

Figure 20 - Situation being examined (with a PID controller)

In the feedforward path we associate, in cascade, a *PID* controller, having transfer function *C(s)*, with the system having the transfer function $G_S(s)$. Then the unity negative feedback loop (unity since the feedback path has no controller whatsoever, i.e. $H(s) = 1$) is closed. Consequently, the overall system will have the following transfer function

$$G_{Sc}(s) = \frac{Y(s)}{R(s)} = \frac{C(s)\,G_S(s)}{1 + C(s)\,G_S(s)} \tag{16}$$

The transfer function *C(s)* depends (cf. expression 11) on the values of the three parameters K_P, T_D and $1/T_I$. However, at least when resorting to the root locus technique, we firstly have to choose the values for T_D and $1/T_I$; in effect, the root locus branches represent the closed-loop poles placement for different values of K_P, ranging from zero to a number as large as we may wish, as we mentioned earlier on. That is why, quite often (and if the *PID* structure is the one depicted in Fig. 5), we personally prefer to rewrite expressions 11 and 16 as follows (note that this is an arguable preference indeed; but, all in all, it is merely a preference)

$$C(s) = C_{PID}(s) = K_P.C_{ID}(s) \quad \text{where} \quad C_{ID}(s) = \frac{T_D\ s^2 + s + 1/T_I}{s} \tag{17}$$

and, hence,

$$G_{Sc}(s) = \frac{Y(s)}{R(s)} = \frac{K_P\ C_{ID}(s)\,G_S(s)}{1 + K_P\ C_{ID}(s)\,G_S(s)} \tag{18}$$

In the four cases illustrated in Fig. 19, we have chosen the following values

		T_D	$1/T_I$
▶	**Case *a)*** [PD - 1 real zero] *(green)*	0.08	0
▶	**Case *b)*** [PI - 1 real zero; 1 pole at origin] *(red)*	0	12.5
▶	**Case *c)*** [PID - 2 real zeros; 1 pole at origin] *(pink)*	0.04	1.25
▶	**Case *d)*** [PID - 2 complex zeros; 1 pole at origin] *(blue)*	0.033	188.5

In Fig. 21 the superimposed root loci for these four cases are shown. Notice that this is a zoomed view, since only the region near the origin is seen; also notice that the *PID* controller

poles and zeros are not shown. In addition, the branches in black correspond to the situation of having $C_{ID}(s) = 1$, that is to say, effectively neither derivative nor integral actions are present; only a proportional gain is available. Again, the root locus for the situation corresponding to the black lines as well as for each one of these four situations are individually shown in figures 22 to 26.

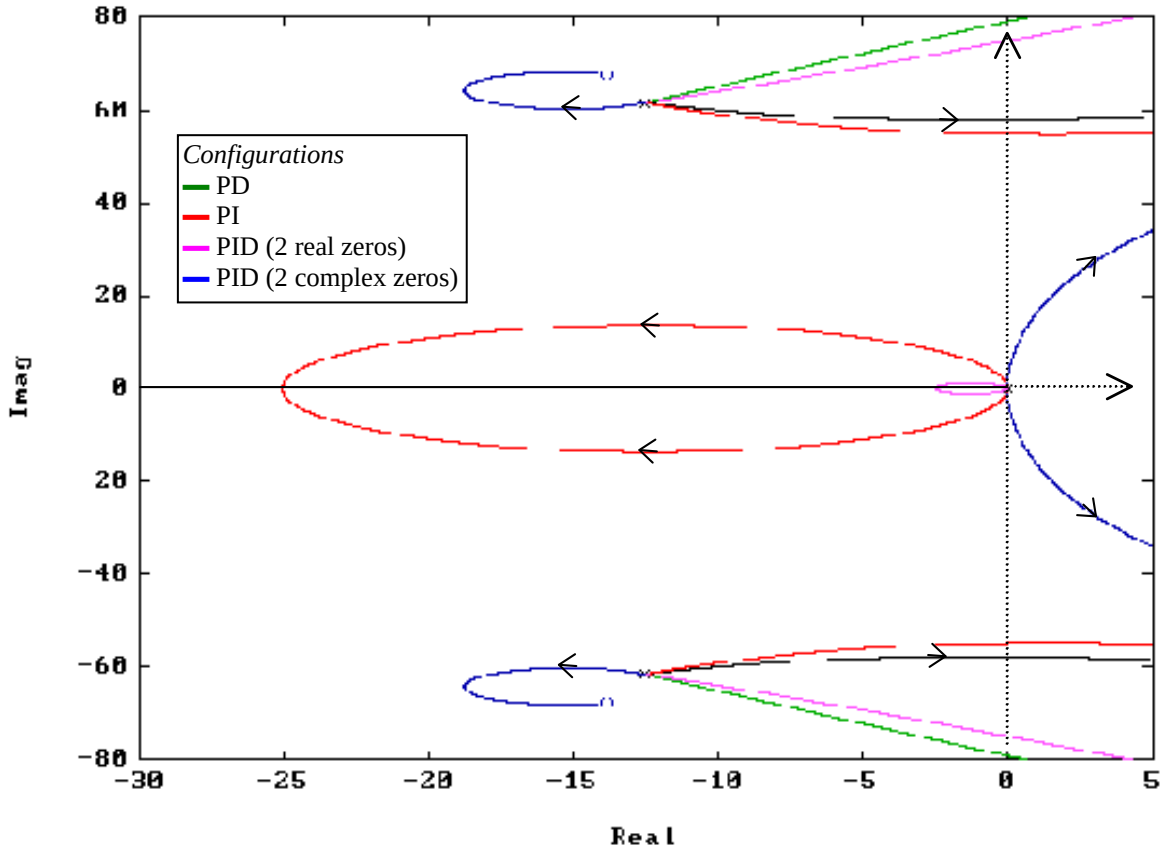

Figure 21 - Superimposed root loci of the four considered cases with PID

By observing Fig. 21, we may say, for the system being considered and mainly aiming to increase its bandwidth, that:

1) The PD approach (case *a*, green lines) seems to be the best one, although the *PID* with 2 real zeros (case *c*, pink lines) allows similar results, both being better than the simplest situation of using only a proportional gain (black lines).

2) The PI approach (case *c*, red lines) is somewhat similar to the simplest one (black lines), even slightly worse.

3) The PID approach with one pair of complex zeros (case *d*, blue lines), aiming at to reach for a near-cancellation of the system dominant complex poles, reveals itself as unacceptable since the resulting control system is inherently unstable.

We must state that a more thorough search for other parameter values could have been carried out. However, in view of the scope of these notes, the choice we made just serves the purpose of pointing up the main effects of using a *PID* controller with a system dynamically characterised by a transfer function like the one of expression 3.

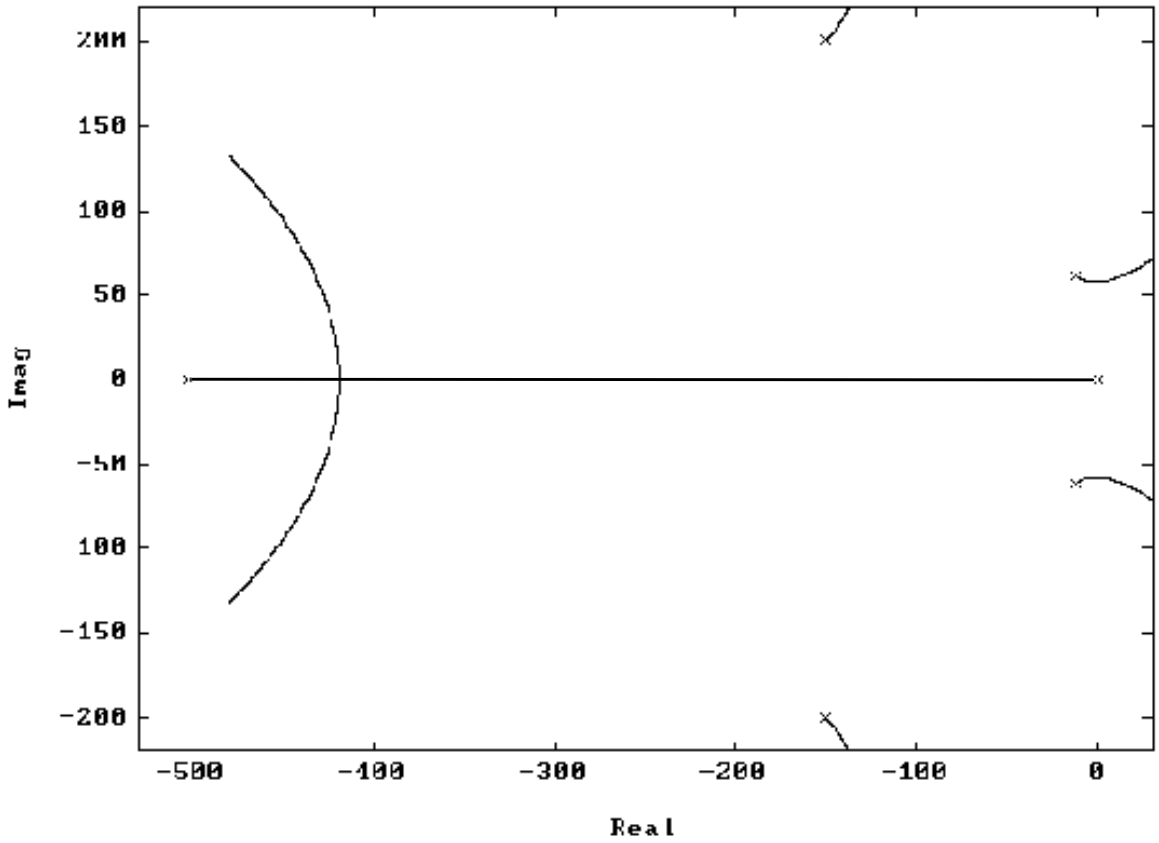

Figure 22 - The simplest case: proportional gain only

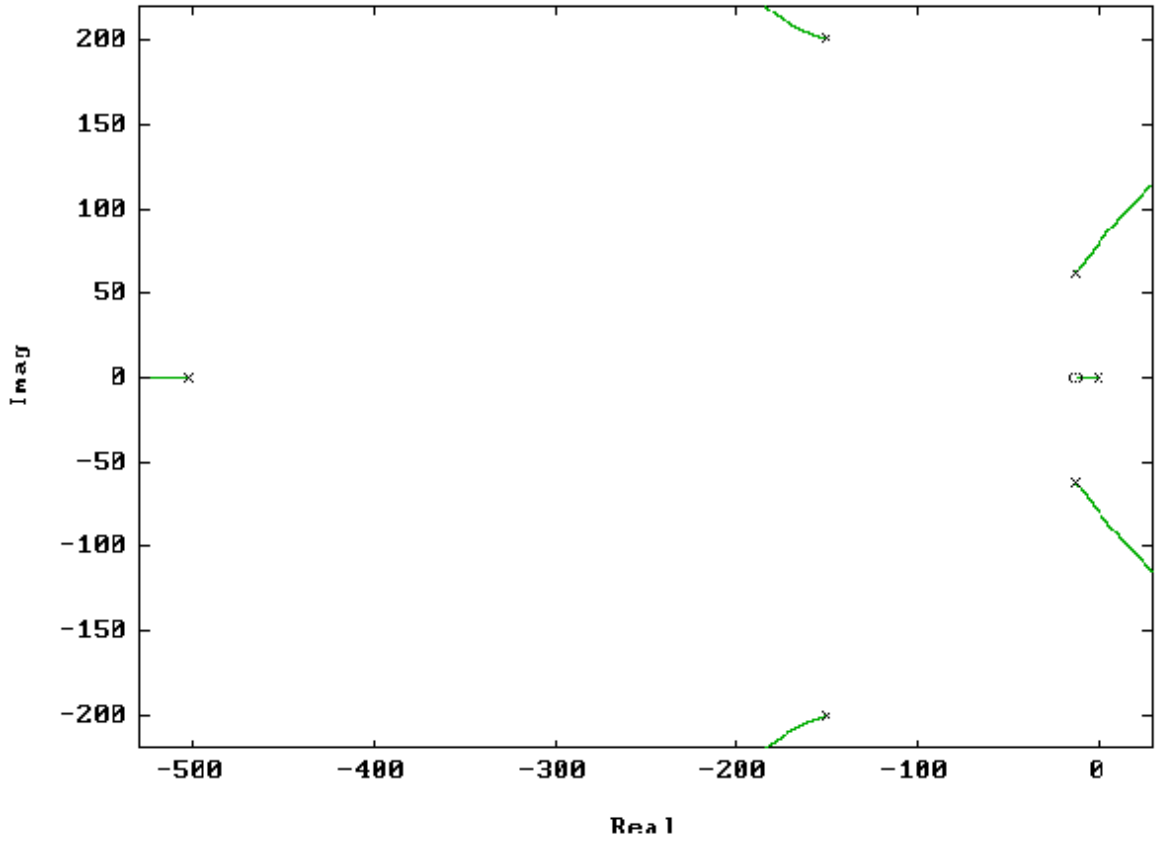

Figure 23 - Case *a*: PD configuration (T_D=0.08)

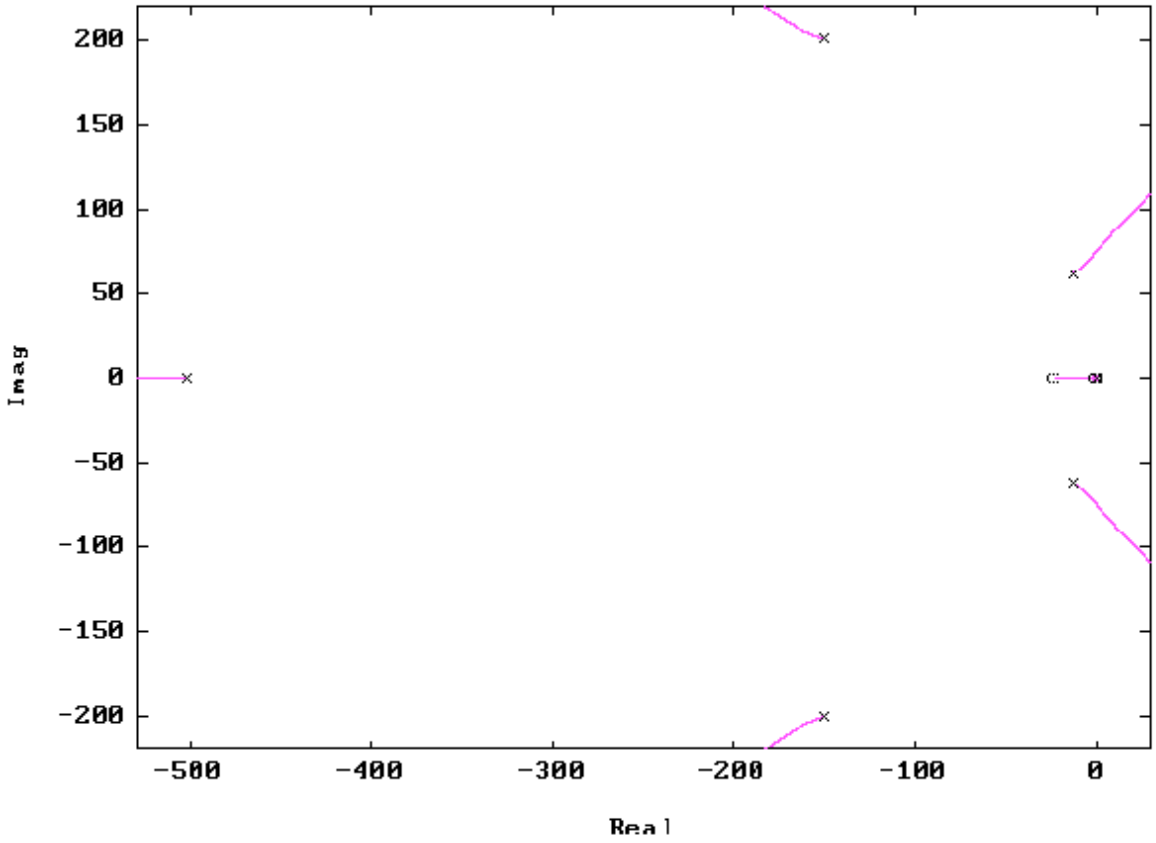

Figure 24 - Case *b*: PI configuration ($1/T_I$=12.5)

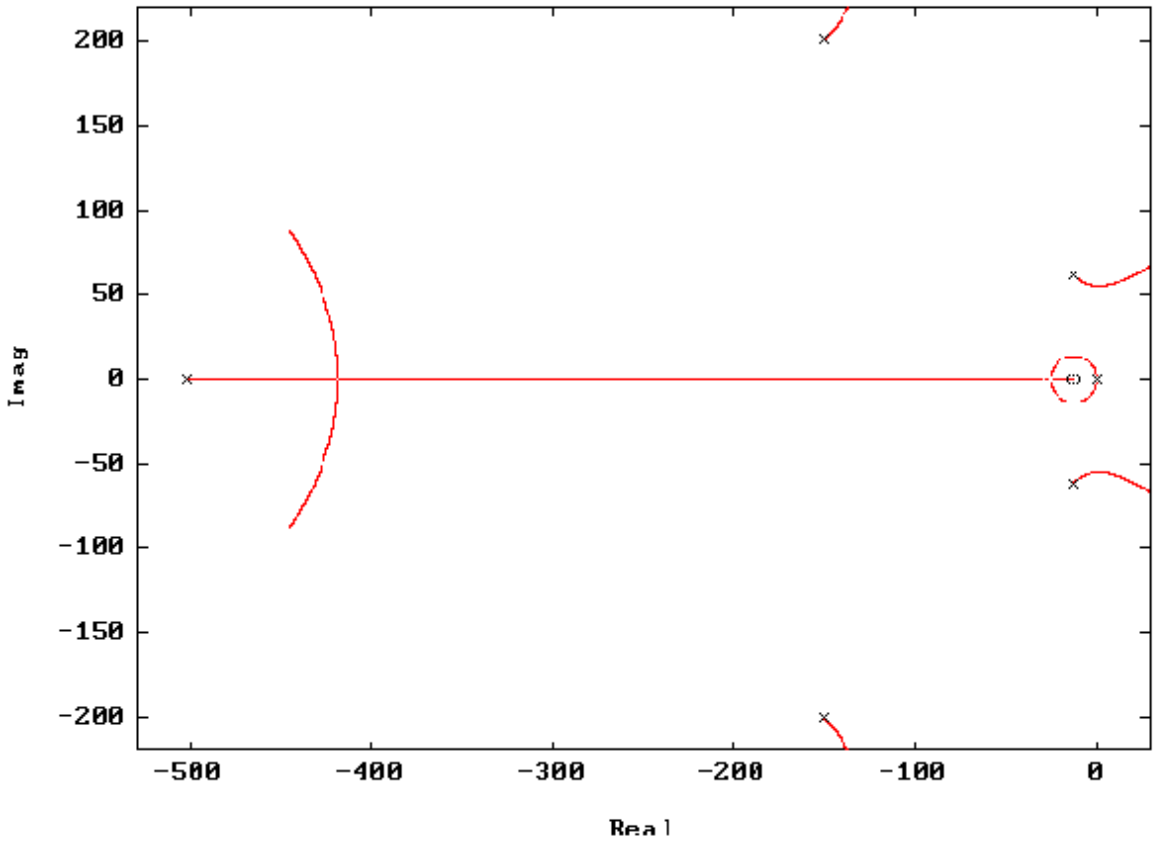

Figure 25~-Case *c*: PID with 2 real zeros (T_D=0.04; $1/T_I$=1.25)

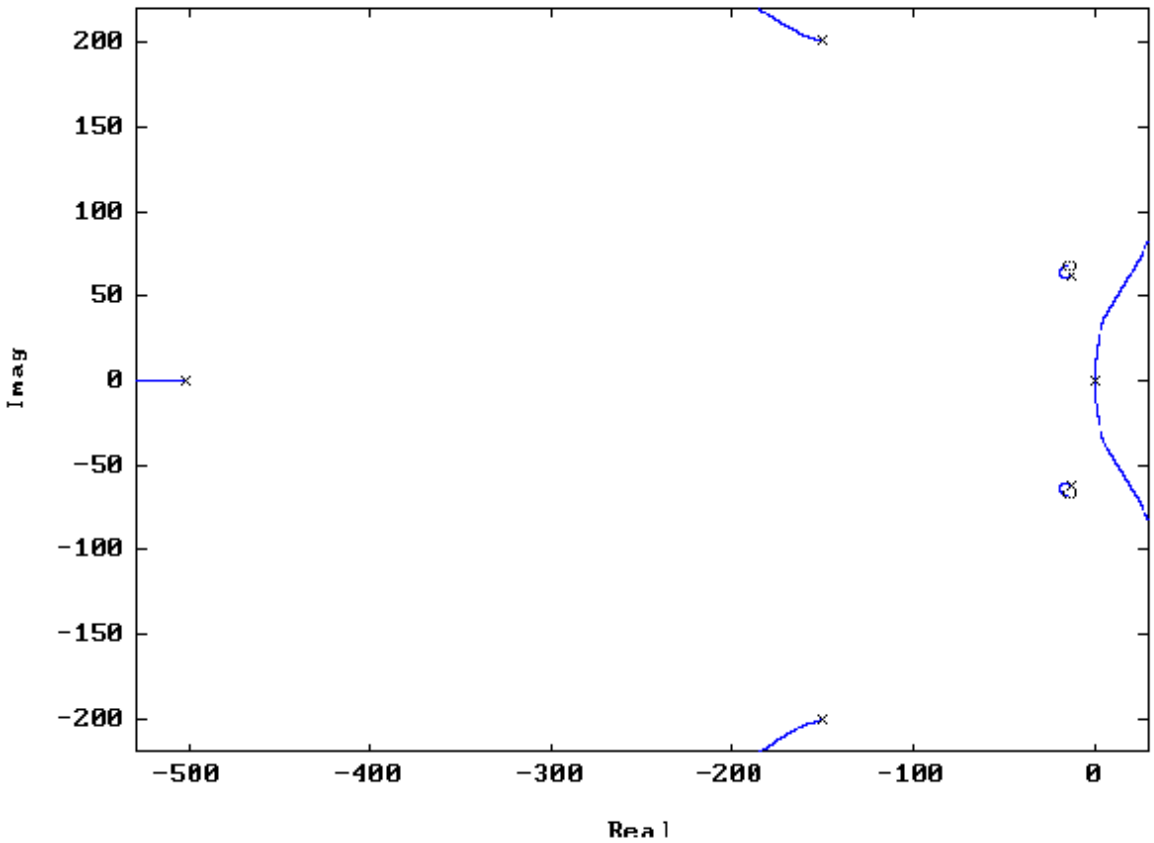

Figure 26 - Case *d*: PID with 2 complex zeros (T_D=0.033; $1/T_I$=188.5)

4.3 - *AAF* and *PID* controllers. Comparison of different situations

So that we can deepen our understanding of the *AAF* and *PID* controllers effects – but now in terms of frequency response as well as of time-response – we shall consider the four cases that are shown in Fig. 27.

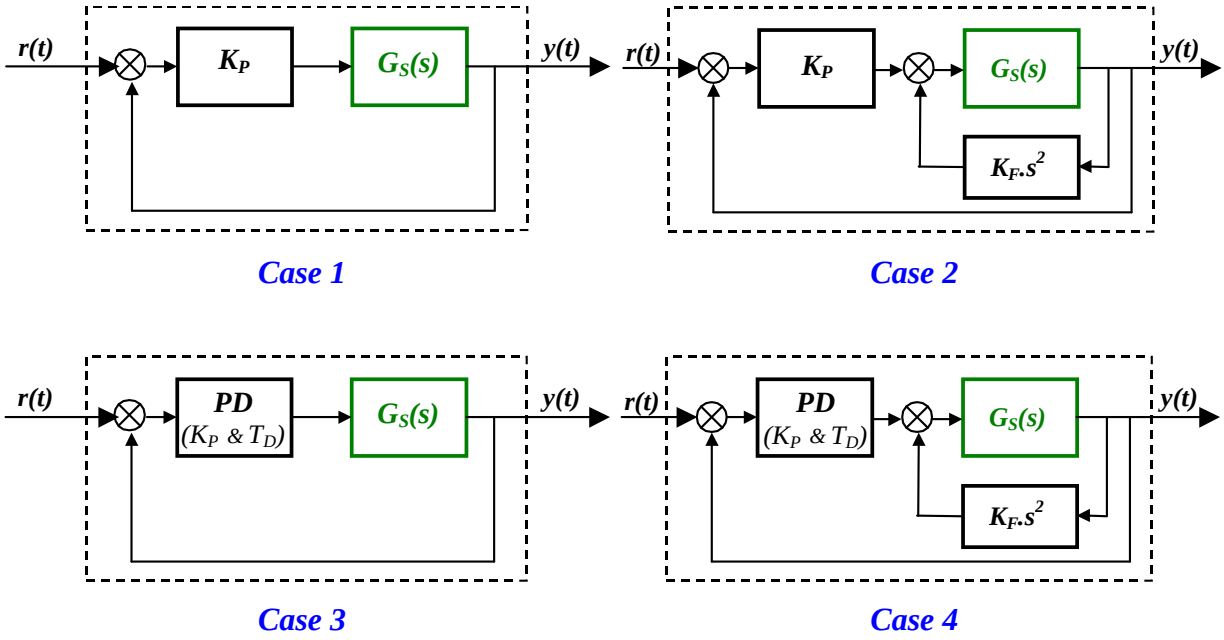

Figure 27 - Cases to be compared

Case 1 – We take again the same system to be controlled, with transfer function $G_S(s)$ given by expression 3, and close an unity feedback loop with a simple proportional gain controller.

Case 2 – We modify $G_S(s)$ by using *AAF*, such that $G_S(s)$ will turn into $G_{Sm}(s)$, and then close an unity feedback loop with a proportional gain controller.

Case 3 – We go back to $G_S(s)$ and then, as in Case 1, we close an unity feedback loop but this time with a PD control action (K_P and T_D).

Case 4 – Finally, we take the situation of Case 2 but we shall resort to a PD control action (K_P and T_D) instead of a proportional gain only.

In these four example cases, we settled for the following parameter values:

		K_P	T_D	K_F
▶	**Case 1** *(red lines)*	10.0	*n/a*	*n/a*
▶	**Case 2** *(blue lines)*	12.5	*n/a*	0.0175
▶	**Case 3** *(pink lines)*	7.5	0.025	*n/a*
▶	**Case 4** *(green lines)*	30.0	0.025	0.0200

In figures 28 and 29 that follows, the frequency response (Bode diagram) and the time-response to an unit step function, respectively, are shown for these four cases. It is important to bear in mind that these responses correspond to closed-loop situations.

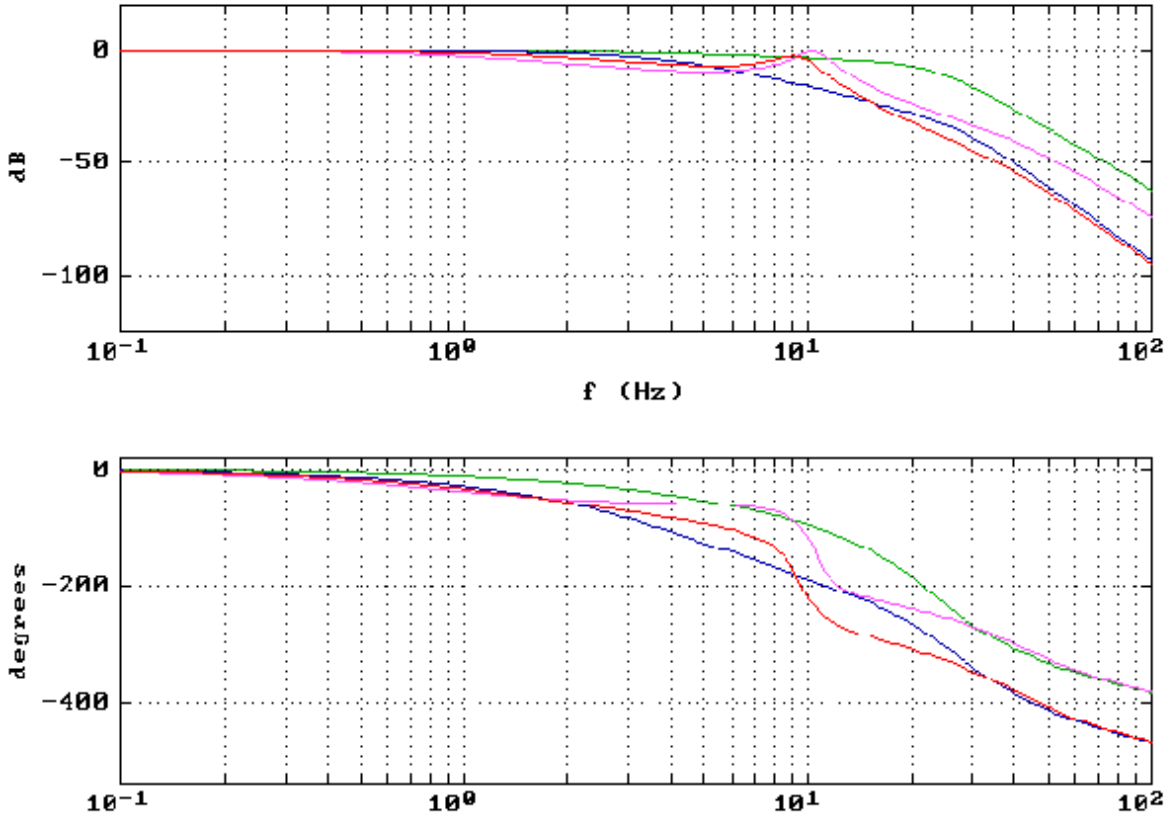

Figure 28 - Frequency response

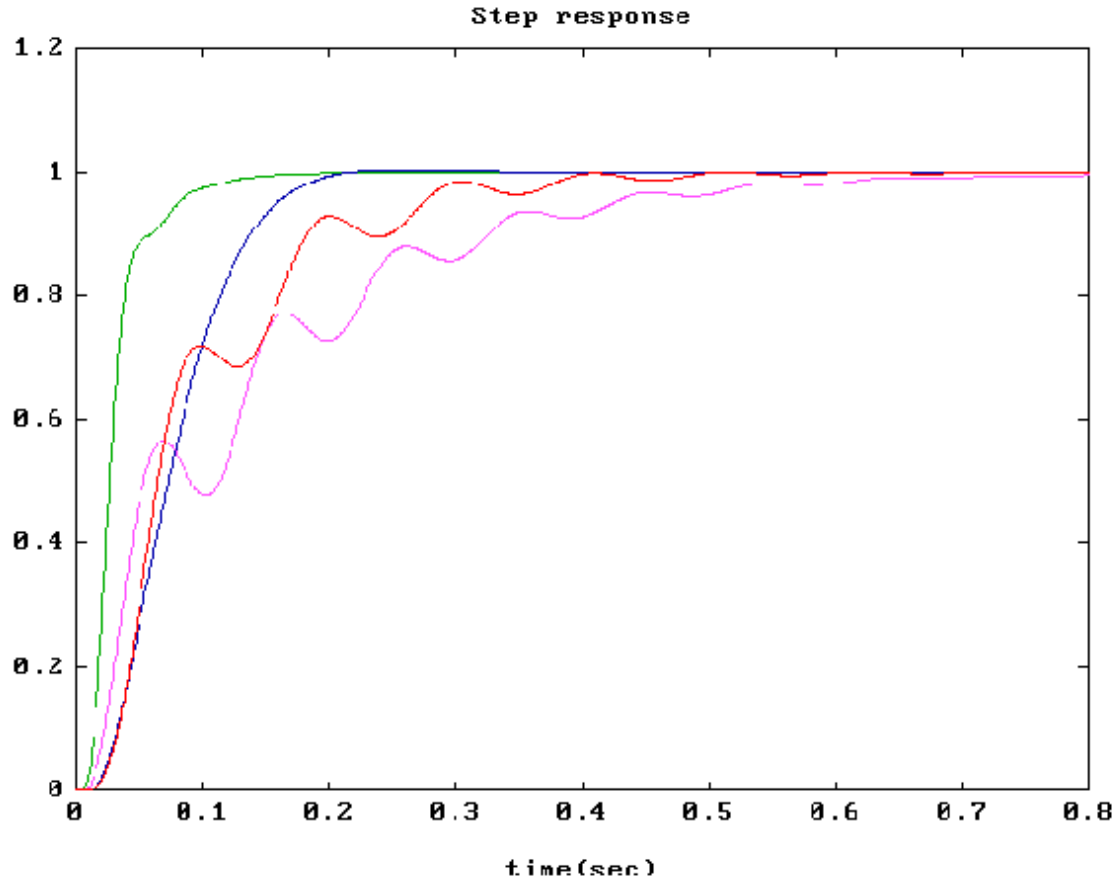

Figure 29 - Time-response to an unit step function

By observing the lines plotted in these two figures we may distinguish that both the responses corresponding to Case 4 are by far the best ones (as we might already expect). Second to these are those corresponding to Case 2, although with a lower bandwidth.

It is important to note that both cases 2 and 4 use the *AAF* controller, and this fact may allow us to draw the following relevant conclusion: for a system like the one we are considering, the exploit of such a controller is crucial and, furthermore, the results will be noticeably better if *AAF* is used in adequate conjunction with a *PID* controller (most probably implementing only a PD control action).

In order to strengthen our understanding on this particular matter, let us recall that we started with the system to be controlled characterised by a transfer function $G_S(s)$ with no zeros and the following six poles (cf. expression 3)

Poles of $G_S(s)$			
real	***imag***	ω_n	ζ
0.00	0.00	0.00	1.00
-12.57	61.56	62.83	0.20
-12.57	-61.56	62.83	0.20
-150.80	201.06	251.33	0.60
-150.80	-201.06	251.33	0.60
-503.00	0.00	503.00	1.00

then we closed the *AAF* control loop setting the value of the auxiliary feedback gain K_F equal to 0.020, thus getting a (new) system having a transfer function $G_{Sm}(s)$ with no zeros and the following six poles (4 real; 1 complex pair)

Poles of $G_{Sm}(s)$ [K_F = 0.02]			
real	***imag***	ω_n	ζ
0.00	0.00	0.00	1.00
-45.94	0.00	45.94	1.00
-61.89	161.29	172.76	0.36
-61.89	-161.29	172.76	0.36
-198.04	0.00	198.04	1.00
-461.96	0.00	461.96	1.00

and, finally, we used a *PID* controller with a PD configuration (K_P = 30.0, T_D = 0.025) and closed the unity feedback loop, thus attaining a system, the servocontrolled system, having a transfer function $G_{Sc}(s)$ with the following six poles (2 real; 2 complex pairs)

Poles of $G_{Sc}(s)$ [K_P = 30.0; T_D = 0.025]			
real	***imag***	ω_n	ζ
-30.04	0.00	30.04	1.00
-58.75	135.31	147.51	0.40
-58.75	-135.31	147.51	0.40
-108.09	25.85	111.14	0.97
-108.09	-25.85	111.14	0.97
-466.00	0.00	466.00	1.00

However, note that, unlike $G_S(s)$ and $G_{Sm}(s)$, the transfer function $G_{Sc}(s)$ has a real zero due to the derivative action; this zero is located at -40.00(= $-1/T_D$).

These successive conceptual steps towards the final control scheme can also be perceived through Fig. 30, where the root loci corresponding to those steps are plotted.

In this figure, the black lines relate to the original system $G_S(s)$, the green ones to $G_{Sm}(s)$ and the blue ones to $G_{Sc}(s)$. The small green dots show the poles location of $G_{Sm}(s)$ for K_F = 0.020; note that, as expected, the blue branches depart from them. Finally, the blue dots show the $G_{Sc}(s)$ poles for a proportional gain K_P = 30.0.

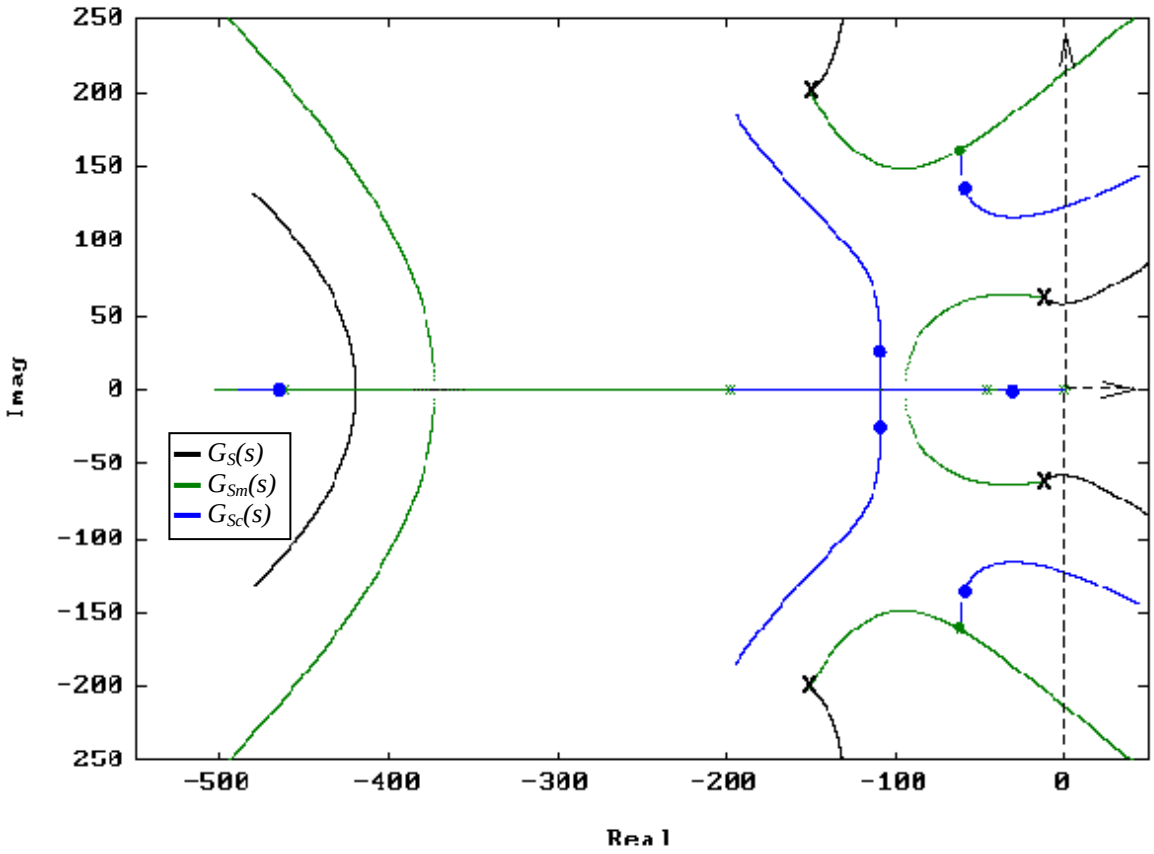

Figure 30 - Root loci corresponding to the conceptual steps

5. Concluding remarks

Hopefully, considering the scope of these notes, it has been shown that, theoretically, in order to fulfil the main goal of increasing bandwidth keeping a reasonable margin of relative stability, the tuning of the INSTRON servocontroller used with the LNEC triaxial seismic shaking table has to rely on the combined use of both the *AAF* and the *PID* controllers, the latter most probably implementing only a PD control action.

As far as we know, when dealing with the tuning of the real servosystem we shall only have direct access to the responses of the system in its closed-loop condition to whatever inputs we may possibly choose. In other words, we shall have only testing access to the dynamical characteristics of $G_{Sc}(s)$. In our opinion, although it would be possible, at least in theory, to carry out specific open-loop tests, this line of attack would be rather complex, difficult, time-consuming and, on top of that, the results would probably fall short of the expectations.

Being so, we consider that the most advisable and feasible approach to the servocontroller tuning procedure should be to perform, in first place, some theoretical calculations – also relying in technical specifications provided by MOOG about the servovalves – aiming at to search out for a "reasonable" transfer function of the system, $G_S(s)$, followed by a theoretical estimation, based on these notes, of the possibly best control parameters (K_F, T_D and K_P), having in mind that these estimates could perhaps be a good starting point to accomplish the real tuning task that we pursue.

Lisbon, LNEC/CIC, October 2003
F. J. Carvalhal

Attachment to

LNEC TRIAXIAL SEISMIC SHAKING TABLE
Notes related with the *tuning* of INSTRON actuator servocontrollers

As mentioned in section 2.1 of the notes main text, most probably the value of ω_S will be lower than the assumed 10 Hz. Thus, for the sake completeness, some results obtained with $\omega_S = 9.42$ rad/s (≈ 1.5 Hz), but with the same damping ratio, $\zeta_S = 0.2$, are presented in this attachment.

For these values of ω_S and ζ_S the system transfer function shall be the following

$$G_S(s) = \frac{(502.65 \times 63165.47 \times 3947.84)}{s\,(s+502.65)\,(s^2+301.59\,s+63165.47)\,(s^2+3.77\,s+88.83)} \qquad (19A)$$

that has no zeros but has the following six poles

0
-502.65
-150.80 + *j* 201.06
-150.80 – *j* 201.06
-1.88 + *j* 9.23 **poles in a**
-1.88 – *j* 9.23 **new location**

The results obtained for this different pair of values will be graphically presented as new figures corresponding to some of the ones shown on the main text (same number followed by a capital A).

Figure in Notes	**Figure in Attachment**	**Characteristic values**
8 *(page 9)*	**8A**	ω_{SV1} = 502.65 rad/s (green) = 325.00 (pink) = 298.74 (blue) = 255.00 (black) = 75.00 (red)
13 *(page 12)*	**13A**	ω_{SV2} = 251.33 rad/s ; ζ_S = 0.6 (green) = 100.00 ; = 0.6 (black) = 19.50 ; = 0.6 (blue) = 12.57 ; = 0.15 (red)
18 *(page 18)*	**18A**	K_F = 0.20 (blue dots) K_F = 0.89 (red dots)
21 *(page 19)*	**21A**	PD config. T_D = 0.35 $1/T_I$ = 0.00 (green) PI config. T_D = 0.00 $1/T_I$ = 2.85 (red) PID config. T_D = 0.35 $1/T_I$ = 0.71 (black) PID config. T_D = 0.265 $1/T_I$ =11.925 (blue)
28 & 29 *(pages 23 & 24)*	**28A & 29A**	Case 1: K_P=2.0 (red) Case 2: K_P=3.0 K_F=0.10 (black) Case 3: K_P=2.0 T_D=0.35 $1/T_I$=0.00 (pink) Case 4: K_P=90.0 T_D=0.35 $1/T_I$=0.00 K_F=0.89 (green)
30 *(page 26)*	**30A**	K_F = 0.89 (small green dots) K_P = 90.0 (blue dots)

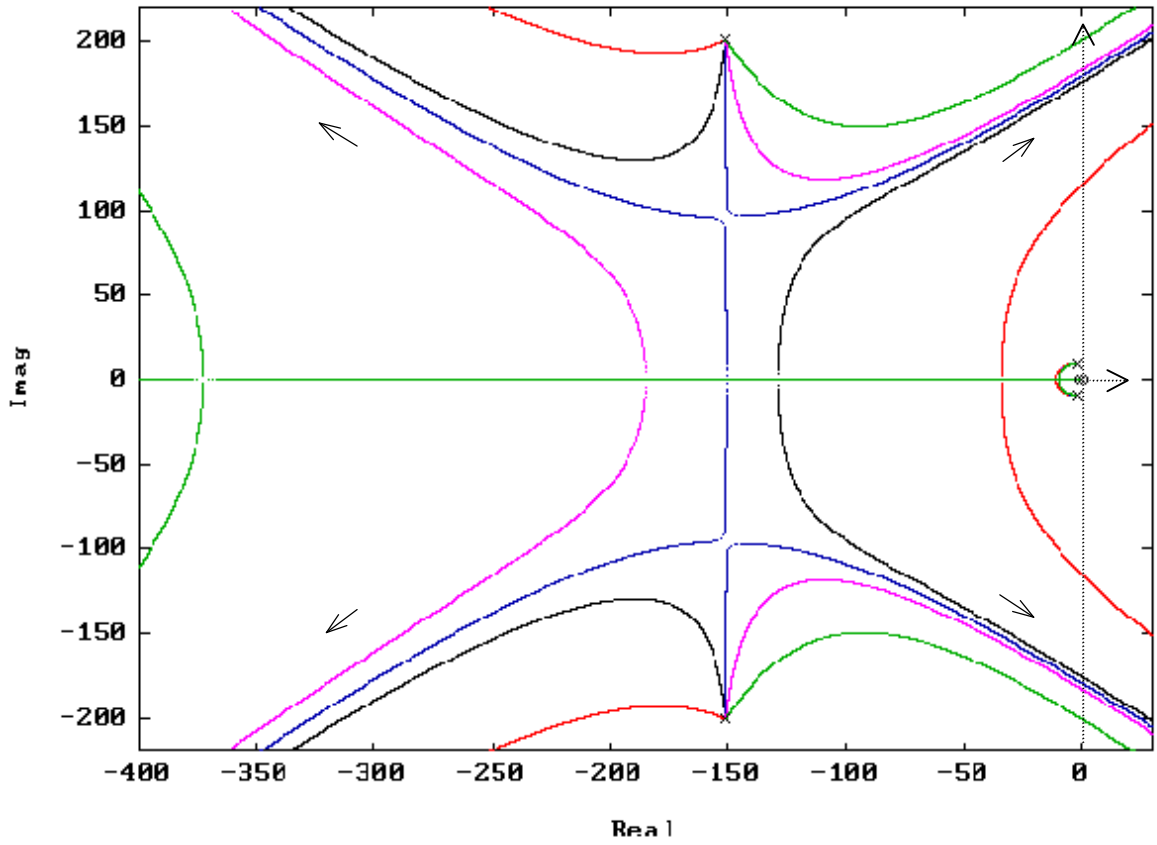

Figure 8A

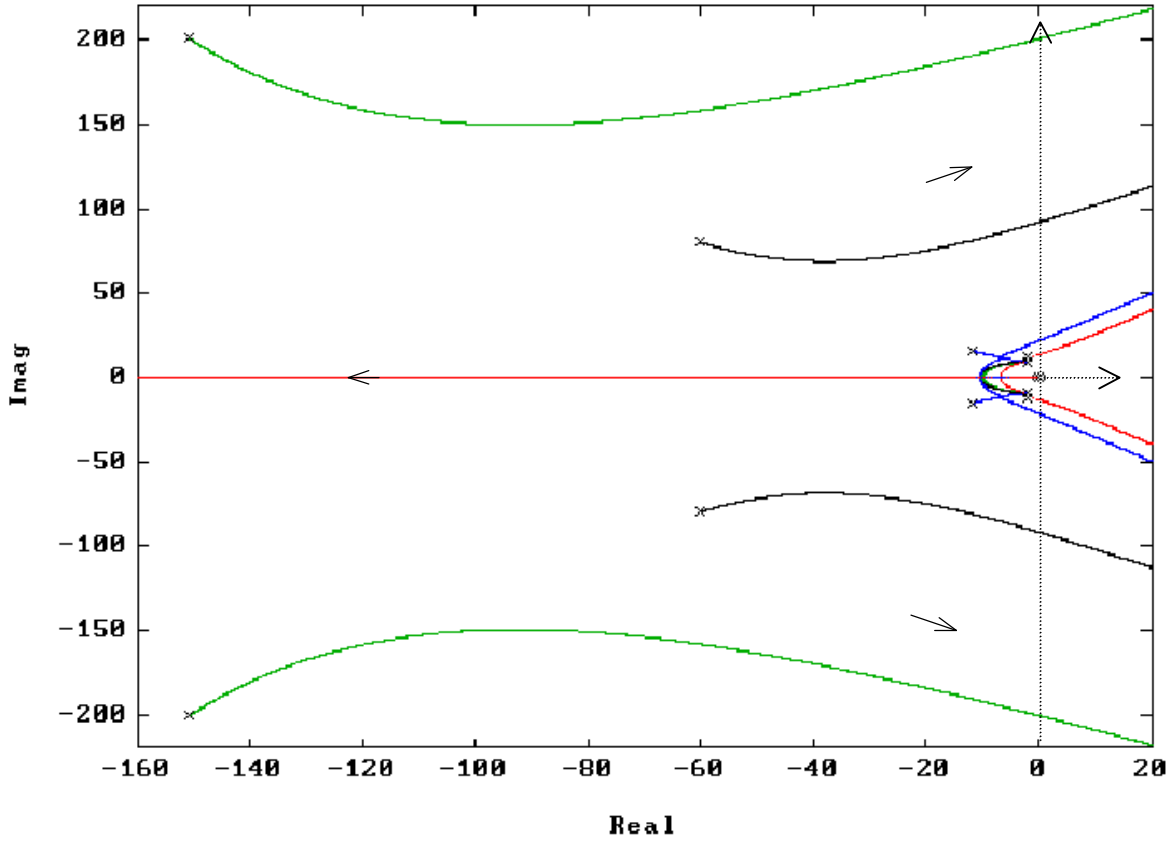

Figure 13A

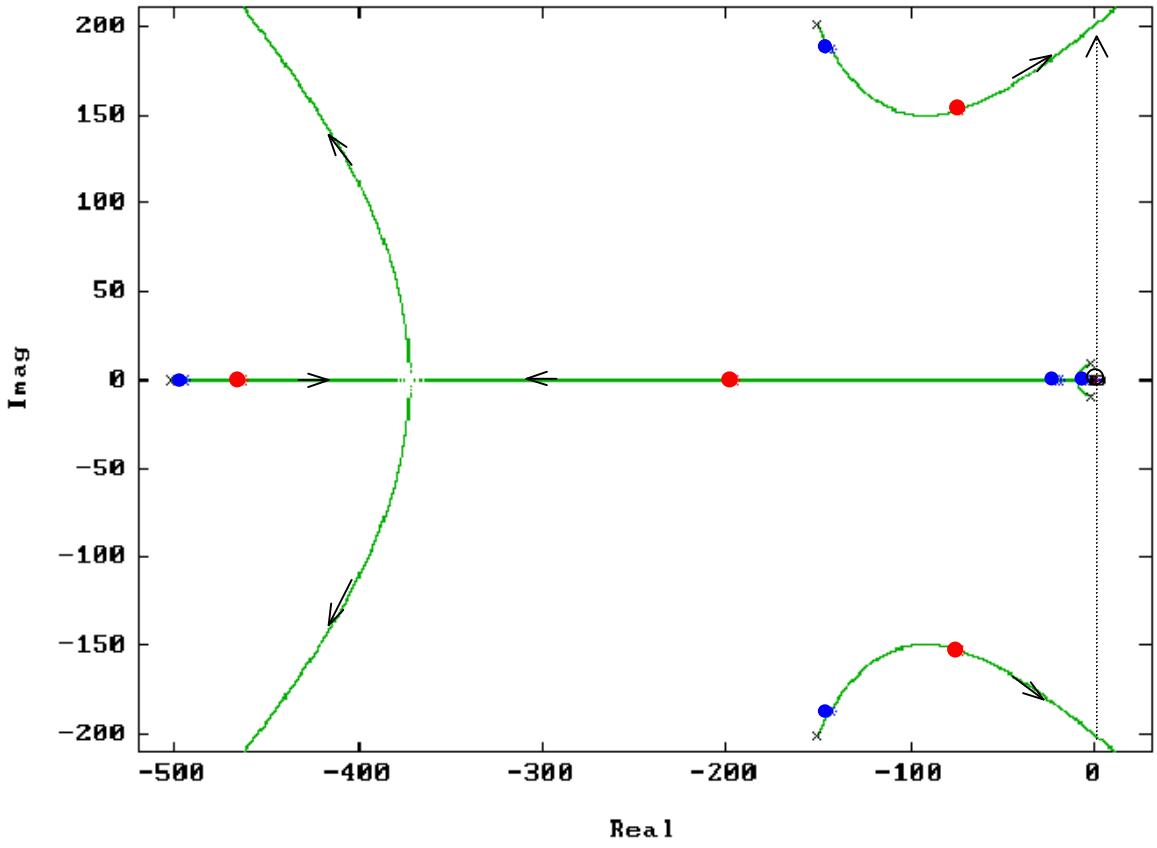

Figure 18A

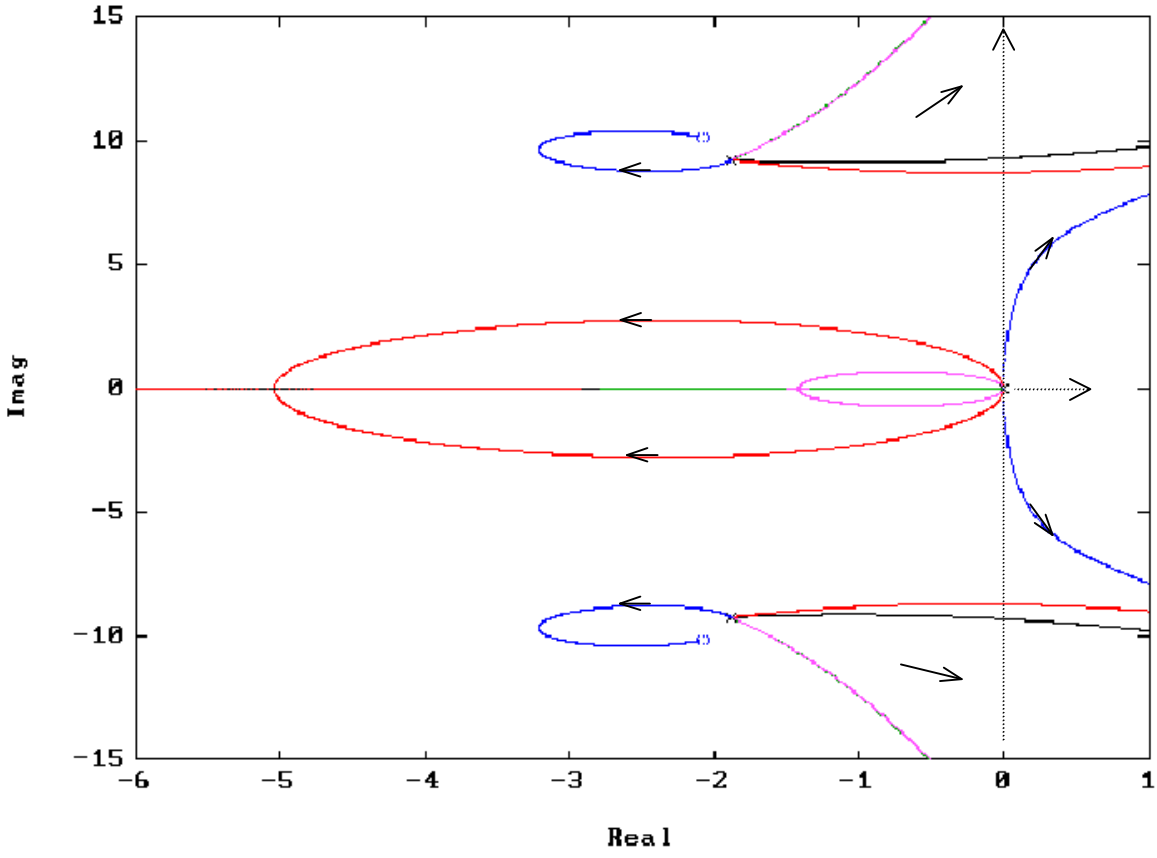

Figure 21A

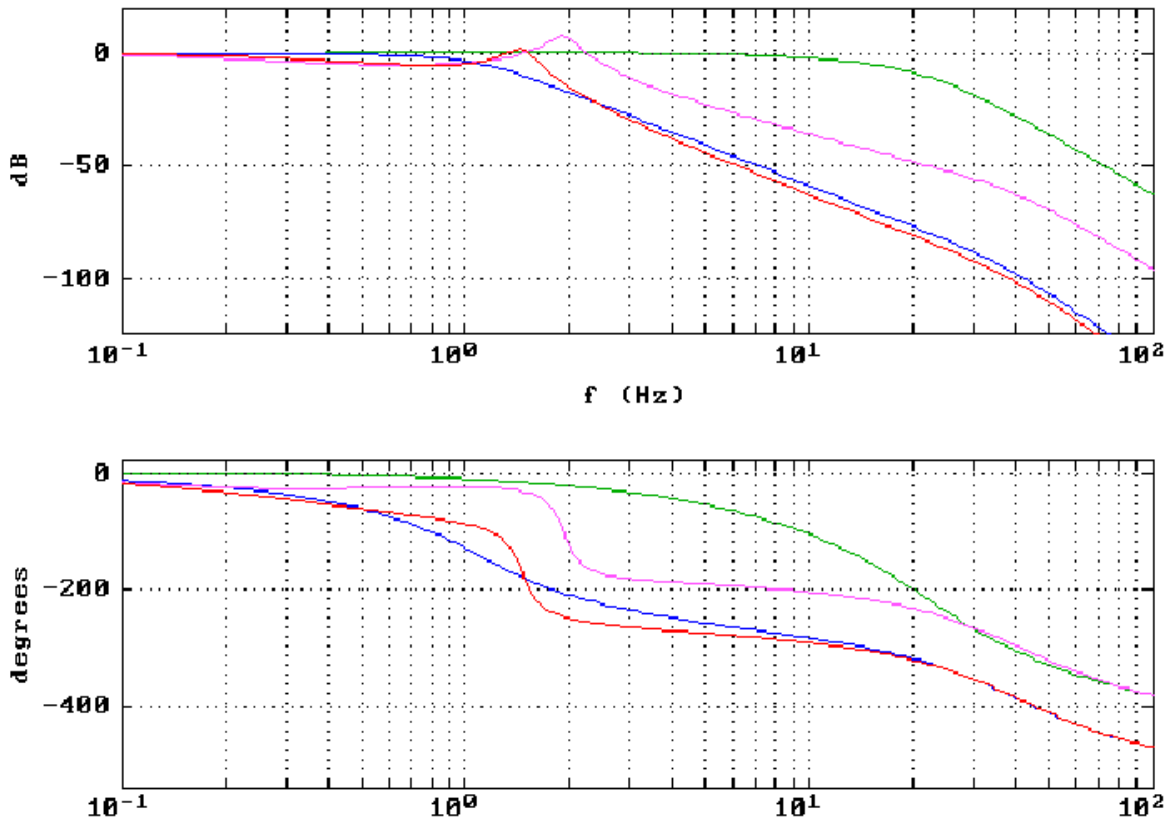

Figure 28A

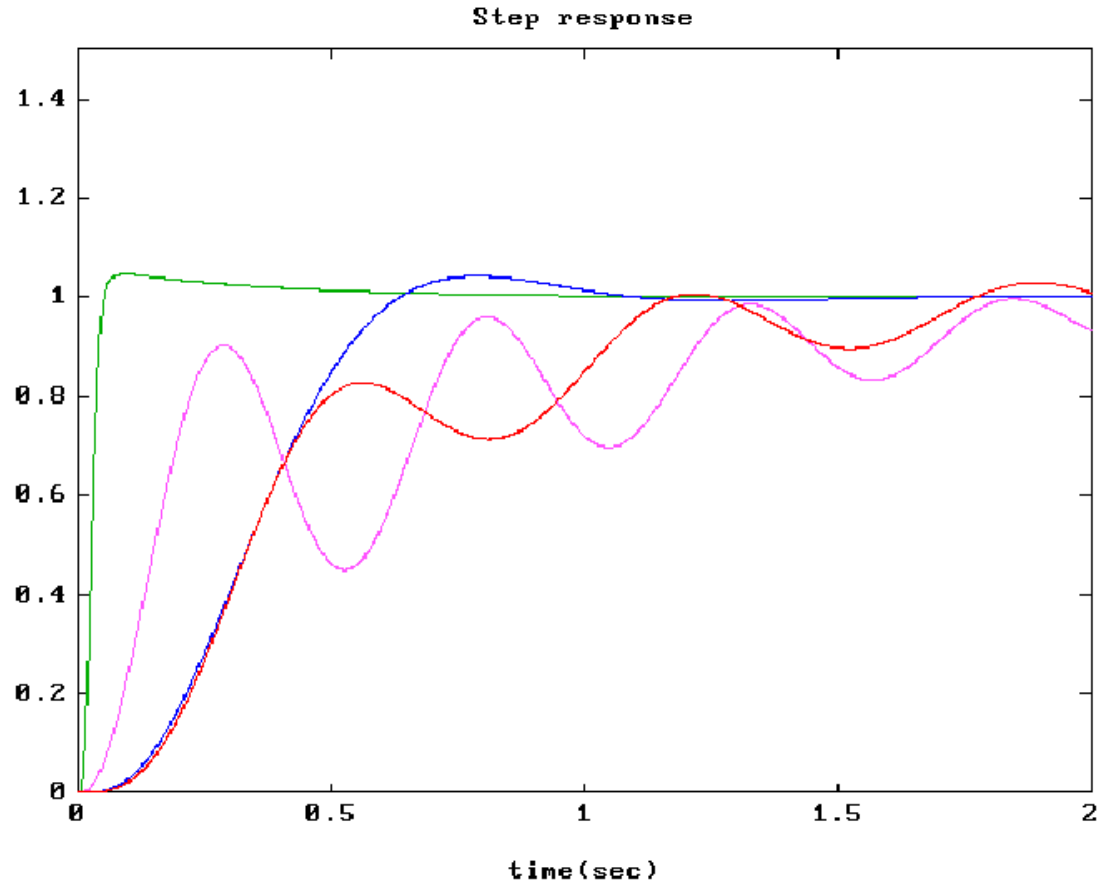

Figure 29A

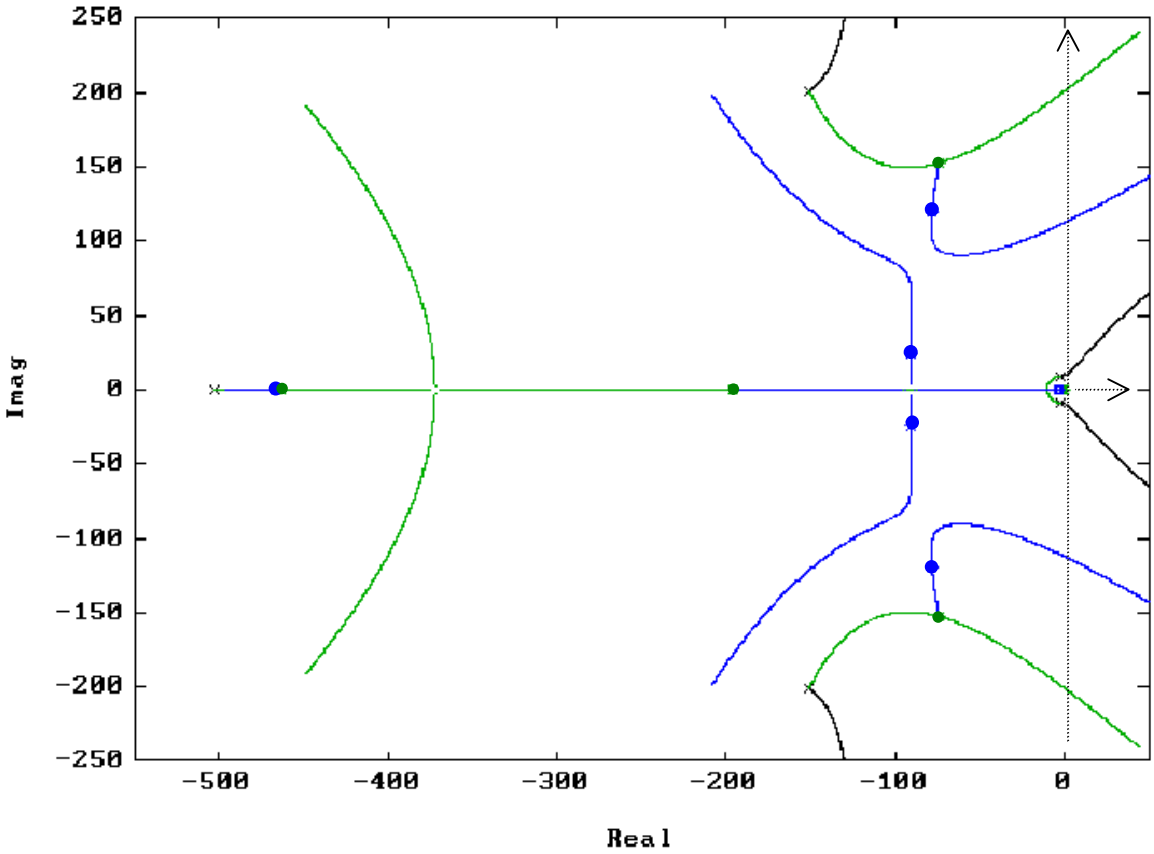

Figure 30A

As a final brief comment, we think that the inspection of the results displayed on this attachment allow us to strengthen the relevant conclusion that was drawn in section 4.3 of the notes main text, that is to say, that for a system like the one we are considering, the exploit of such an *AAF* controller is crucial and, furthermore, that the performance of the servocontrolled system will be noticeably better if the *AAF* controller is used in adequate conjunction with a *PID* controller

■

LNEC, October 2003